L1 retrotransposition assay) or 0.3 μg of the neo^r-based *Alu* expression vector pYa5neotet and 0.1 μg of the L1 ORF2 expression plasmid pBudORF2opt (for the *Alu* retrotransposition assay) using Lipofectamine and Plus reagents (Invitrogen). As a negative control, 0.5 μg of a GFP expression vector, pCA-EGFP, was transfected into HeLa cells. After 72 h, the cells were trypsinized, re-seeded into T25 or T75 flasks for G418 selection (1 mg/ml for the L1 assay and 400 μg/ml for the *Alu* assay), and maintained. At 14 days after selection, the resultant G418-resistant (G418^R) colonies were fixed, stained with crystal violet (Merck), and counted.

Oligomerization assay

To perform a coimmunoprecipitation-based oligomerization assay, plasmids (0.5 μg) expressing HA-tagged wild-type and mutant hA3G were transfected along with phA3G-myc (0.5 μg) into 293T cells using FuGENE 6. After 48 h, the transfected cells were suspended in 500 μl of RIPA buffer (50 mM Tris-HCl, pH 7.4, 150 mM NaCl, 1% NP-40, 0.5% sodium deoxycholate, 0.1% SDS, complete protease inhibitor cocktail [Roche]). The resultant lysates were clarified by brief centrifugation, pre-cleared with 30 μl of Protein A-Agarose Fast Flow (GE Healthcare) for 1 h at 4°C, and then incubated with an anti-myc affinity gel (Sigma). After 1 h at 4°C, the immune complexes were extensively washed with RIPA buffer. Equal aliquots of the total and bound fractions were subjected to gel electrophoresis and transferred to a nitrocellulose membrane. The membranes were probed with an anti-HA mouse monoclonal antibody (Sigma) or an anti-β-actin mouse monoclonal antibody (AC-74, Sigma). The signal intensities of the immunoprecipitated hA3G protein on Western blots were quantified using the LAS-3000 imaging system (Fujifilm). For the RNase A treatment experiment, the immune complexes were separated into two aliquots. The wild-type sample was incubated with or without 25 U of RNase A (Sigma) at room temperature for 30 min. Samples were extensively washed and then resuspended in loading dye. The samples were assayed as described above.

Molecular modeling of the head-to-head dimer structure of the N-terminus of hA3G

Head-to-head dimer models of hA3G N-terminal domain were obtained by homology modelling using either the crystal structure of human APOBEC2 (hA2) at a resolution of 2.50 Å or the NMR structure of the C-terminal domain of hA3G (PDB code: 2NYT chain A [56] or 2JYW [57], respectively) as a template, as previously performed [34,58-60]. To minimize misalignments between the hA3G N-terminal domain as a target sequence and either hA2 or the C-terminal domain of hA3G as a template sequence, we used the multiple sequence alignment method with the sequences of hA3A (GenBank accession number: NM_145699), hA3C (GenBank accession number: NM_014508), and hA3F (GenBank accession number: NM_145298). Multiple sequence alignments were generated using 'MOE-Align' in Molecular Operating Environment (MOE) version 2010.10 (Chemical Computing Group Inc., Quebec, Canada). Three-dimensional (3-D) models of the hA3G N-terminal domain were constructed by the homology modeling technique using 'MOE-Homology' in MOE as previously described [61]. We obtained 25 intermediate models per homology modeling session in MOE, and we selected the 3-D models that were intermediate models with best scores according to the generalized Born/volume integral methodology [62]. The 3-D structure was thermodynamically optimized by energy minimization using MOE and an AMBER99 force field [63] combined with the generalized Born model of aqueous solvation implemented in MOE [64]. The physically unacceptable local structure of the optimized 3-D model was further refined based on the evaluation of the Ramachandran plot using MOE.

Results

hA3 family members differentially inhibit Alu retrotransposition

To determine if hA3 family members are able to inhibit *Alu* retrotransposition as well as L1 retrotransposition [37], we performed a neo^r-based retrotransposition assay [5]. In this assay system, we utilized a L1 ORF2 expression plasmid that is required for *Alu* retrotransposition [53], together with an *Alu* clone DNA carrying a reverse-oriented neo^r gene separated by a gamma-globin intron. After transfection of the cells with this construct, neo^r with *Alu* is transcribed, spliced, reverse-transcribed, and integrated. Then, the neo^r gene that is integrated with *Alu* is driven by the CMV promoter and expressed. After G418 selection following transfection, we were able to quantify the retrotransposition level by counting the number of G418^R colonies. hA3 protein expression in the cells were confirmed by immunoblotting using anti-HA antibodies (Figure 1A). Without the co-expression of an hA3 protein, *Alu* retrotransposition occurred at the level shown in the upper left panel of Figure 1B. In contrast, the co-expression of any of the hA3 proteins differentially inhibited *Alu* retrotransposition, and in particular, the expression of hA3A, hA3B, or hA3G strongly decreased the transposition level of *Alu* elements (Figure 1C). Thus, we conclude that hA3 proteins act to differentially suppress *Alu* retrotransposition. Importantly, in agreement with previous reports [34-36,39], we observed that hA3G has an inhibitory effect on *Alu* retrotransposition in the assay. It should be noted that these activities against *Alu* correlated exactly with the patterns previously observed for the inhibition of L1 [37].

The *N*-terminal 30 amino acids of hA3G determine the inhibitory effect on Alu retrotransposition

Because hA3G is the best characterized hA3 family member protein, we focused on this protein and attempted to determine the region responsible for its anti-retrotransposon activities. To identify the relevant region, we created a series of mutants with serial deletions from the N-terminus up to amino residue 150 (Figure 2A). Protein expression in the cells transfected with each plasmid was confirmed by immunoblotting using an anti-HA antibody (Figure 2B). hA3G mutants lacking the C-terminal domain were undetectable as previously reported [34,65] and therefore could not be used for further experiments. Immunofluorescence microscopy confirmed that hA3G deletion

Oligomerized hA3G inhibits retrotransposition

Figure 1

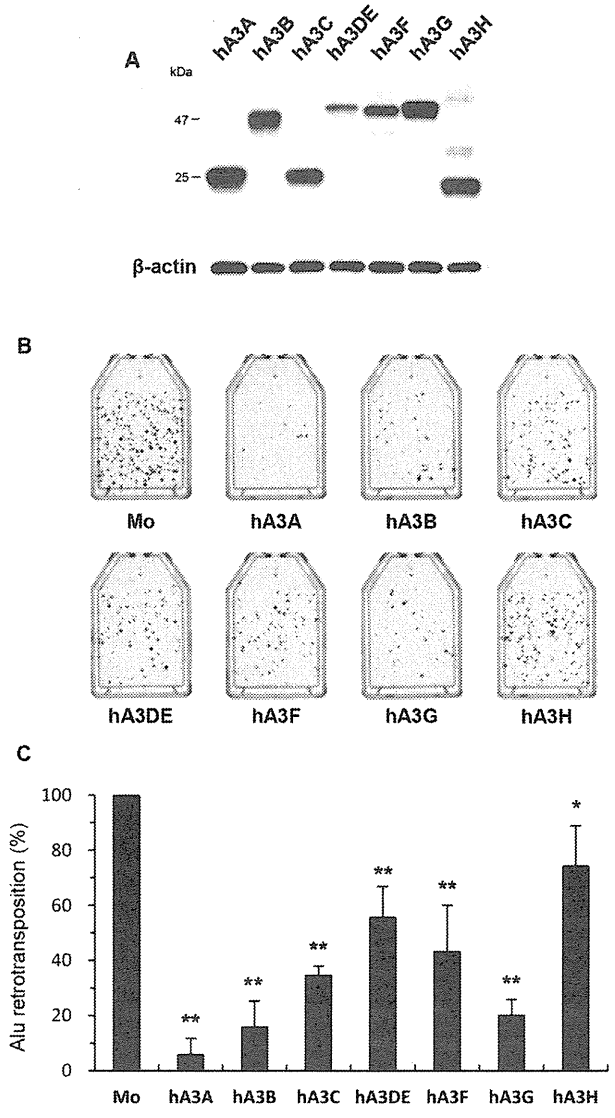

Figure 1. hA3 proteins inhibit Alu retrotransposition at differential levels. (**A**) Western blot analysis was performed by using extracts from 293T cells transfected with HA-tagged hA3 expression plasmids. Antibodies specific for HA were used. (**B**, **C**) HeLa cells were cotransfected with the *neo*^{r}-based *Alu* expression vector pYa5neotet and the L1 ORF2 expression plasmid pBudORF2opt, together with the respective hA3 expression plasmid. Seventy-two hours later, the cells were trypsinized, re-seeded into T25 or T75 flasks, and subjected to G418 (400 μg/ml) selection. At 14 days after selection, the resultant G418^R colonies fixed, stained with crystal violet (B), and counted to determine the level of *Alu* retrotransposition (C). The retrotransposition level in the absence of hA3 proteins was set to 100%. The data shown are the mean ± SD of triplicate experiments. Mo, mock. *$P < 0.05$, **$P < 0.005$, *t*-test.

doi: 10.1371/journal.pone.0084228.g001

mutant proteins other than NΔ150 were predominantly localized to the cytoplasm, as was the wild-type protein (Figure 2C). These deletions also abrogated the anti-HIV-1 activity of hA3G (Figure S1). We performed an *Alu* retrotransposition assay by transfecting HeLa cells with the *Alu* expression plasmid, the L1 expression plasmid, and a wild-type or mutant hA3G plasmid, and we observed that the deletion of 30 or more residues from the N-terminus of hA3G completely abrogated the inhibitory activity of hA3G on *Alu* retrotransposition (Figures 2D and 2E). We therefore conclude that the N-terminal 30 amino acids of hA3G are critical for the inhibition of *Alu* retrotransposition.

The inhibitory effect of hA3G on Alu retrotransposition is associated with its oligomerization and is independent of its deaminase activity

The anti-HIV-1 activity of hA3G is known to be dependent on two different activities, deamination and oligomerization, the former of which has been shown to be disrupted by the mutation of E259 located in the C-terminal cytidine deaminase (CD2) [65,66], and the latter of which has been reported to be abrogated by the mutation of C97 and C100 located in the N-terminal cytidine deaminase (CD1) [65]. Based on these past findings, we wished to determine which functions of hA3G are crucial for blocking the ability of *Alu* to retrotranspose. We created plasmids expressing hA3G defective in either oligomerization or deamination (C97/100A or E259Q, respectively; Figure 3A) and confirmed the expression of these proteins by immunoblotting using an anti-HA antibody (Figure 3B). Interestingly, the *Alu* retrotransposition assay revealed that the C97/100A oligomerization mutant of hA3G had no inhibitory activity against *Alu* retrotransposition, whereas the E259Q deamination mutant retained wild-type activity (Figure 3C). These observations confirmed the previous results [34,35], showing that the inhibition of *Alu* retrotransposition by hA3G is not due to the ability of hA3G to deaminate this retrotransposon but is due to its ability to form an oligomer.

The *N*-terminal 30 amino acids of hA3G are required for the oligomerization of this protein

Because hA3G's inhibitory activity against *Alu* retrotransposition was abolished in the mutants carrying an N-terminal deletion of 30 or more residues (Figure 2) and in the oligomerization mutant harboring mutations at amino acid positions 97 and 100 (Figure 3), we reasoned that the N-terminal 30 amino acids of hA3G might be critical for its ability to form oligomers. To test this hypothesis, we performed an oligomerization assay by coexpressing wild-type hA3G tagged with Myc and the mutant hA3Gs tagged with HA. The cell lysates were then immunoprecipitated with an anti-HA antibody and immunoblotted with an anti-Myc antibody. As shown in Figure 4, the E259Q deamination mutant of myc-tagged hA3G was efficiently coimmunoprecipitated with the HA-tagged wild-type protein. In contrast, the N-terminal serial deletion mutants lacking 30 or more residues completely lost the ability to oligomerize, as did the C97/100A mutant. When the immunoprecipitated samples were treated with RNase A, the oligomerization efficiency of hA3G was moderately decreased (Figure S2), consistent with the previous reports that cellular RNA might contribute to the stabilization of hA3G's oligomer [34]. Thus, the 30 amino acids at the N-terminus of hA3G are responsible for its oligomerization.

The *N*-terminal 30 amino acids of hA3G are the structural key for its oligomerization

To fully understand the mechanism by which N-terminal 30 amino acids of hA3G regulate oligomerization, we analyzed the effect of the deletion of the N-terminal 30 amino acids on the predicted 3-D structure of the hA3G dimer that was reported to be the major form of hA3G oligomer [34,59]. Thermodynamically stable N-terminal structures of wild-type hA3G and its N-terminal 30-amino-acid deletion mutant were constructed by homology modeling using the hA2 crystal structure as a template. As shown in Figures 5A and B, when the structures of the wild-type and deletion mutant hA3G proteins were compared, it was obvious that the N-terminal 30 amino acids (shown in cyan in Figure 5A) were present along the contact surface of the hA3G dimer, and therefore, the deletion of this region could abolish the interaction interface between the two hA3G molecules. We thus conclude that the N-terminal 30 amino acid residues of hA3G are located at the dimer interface and are critical for oligomerization.

Residues 24–28 contribute to the ability of hA3G to homooligomerize and inhibit Alu retrotransposition

Next, we analyzed the interaction interface of the hA3G dimer by structural modeling based not only on the hA2 crystal structure but also on the C-terminal hA3G (hA3G-C) NMR structure in parallel. Both structural modeling of wild-type hA3G revealed that, among the N-terminal 30 amino acids, a cluster of dimer interface residues (R24, P25, I26, L27, and S28) located in the N-terminal core structure α1-loop-β1 of hA3G interact with the counterpart residues of another monomer (Figures 6A and 6B). Importantly, this interface corresponds structurally (but not genetically) to a part of the potential oligomerization interfaces of the hA3G C-terminal domain, as described by Shandilya et al. [67]. At this putative interaction surface (Figures 6A and 6B), R24 likely interacts with D130 of another monomer through hydrogen bonds and electrostatic interactions, whereas the isoleucine/leucine residues at positions 26/27 can form a hydrophobic interaction with the counterpart residues of another monomer. hA2-based modeling shows that the serine residue at position 28 forms another hydrogen bond with the counterpart residues of another monomer (Figure 6A), although the same residue in hA3G-C-based modeling appears to be slightly separated from the counterpart residue of another monomer (Figure 6B). Additionally, the structural stability would be enhanced by a proline residue at position 25 in the loop. Thus, we speculated that the mutation of these residues might abolish the oligomerization of hA3G. To test this hypothesis, we first addressed whether structural modeling would be able to distinguish oligomerization-deficient and oligomerization-intact hA3Gs by analyzing the model of an hA3G mutant (hA3G-4G(124–127)), in which we introduced the small amino acid glycine in place of the aromatic amino acid residues

Oligomerized hA3G inhibits retrotransposition

Figure 2

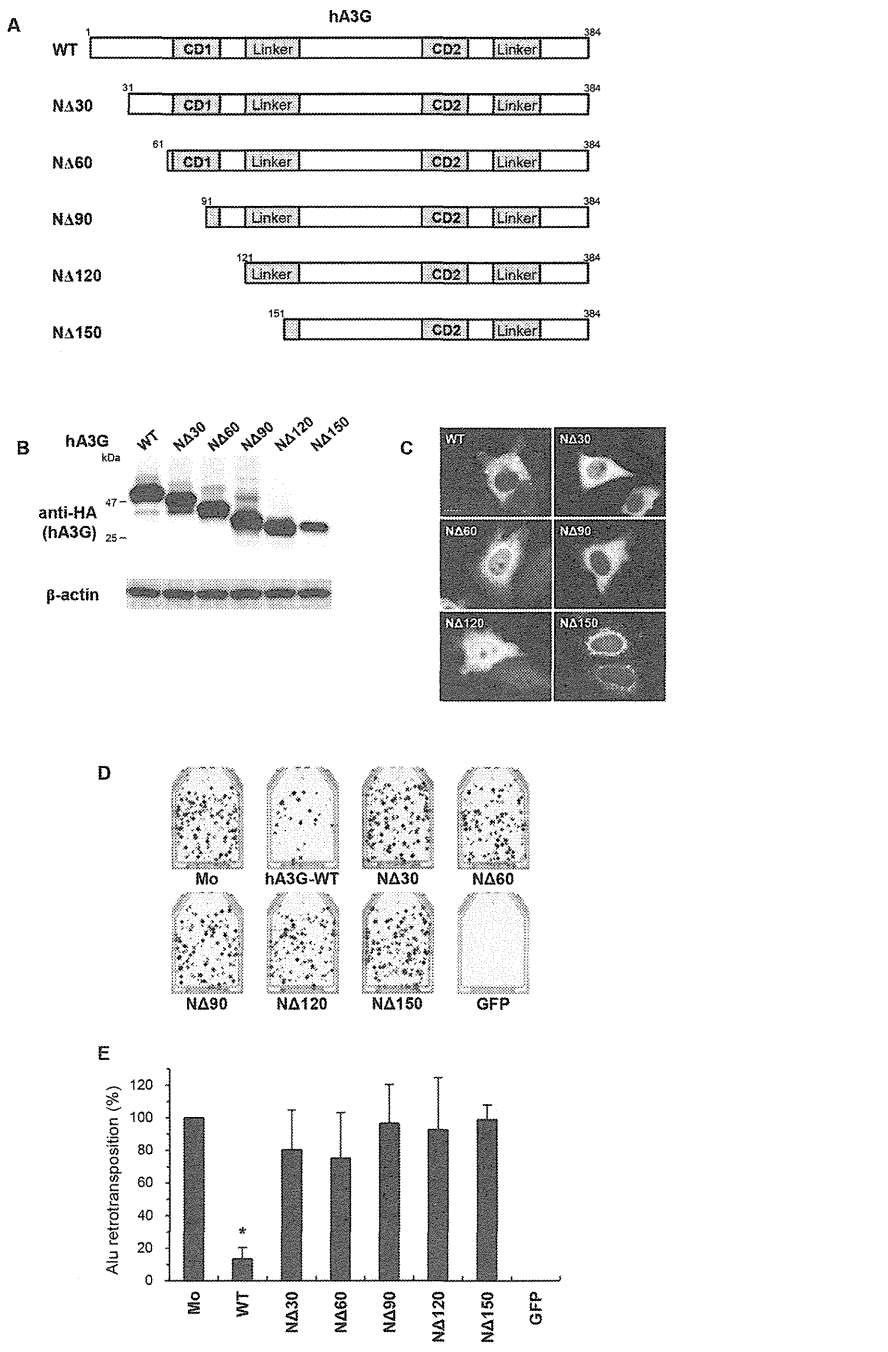

Figure 2. The N-terminal 30 amino acids regulate the anti-Alu activity of hA3G. (**A**) Schematic depiction of a series of N-terminal deletion mutants of hA3G. CD1, N-terminal cytidine deaminase; CD2, C-terminal cytidine deaminase. (**B**) Western blot analysis was performed using extracts from 293T cells transfected with plasmids expressing HA-tagged hA3G mutant proteins. Monoclonal antibodies specific for HA (upper) or β-actin (lower) were used. (**C**) Representative images of HeLa cells transfected with the indicated plasmids are shown. hA3G wild-type (WT), NΔ30, NΔ60, NΔ90, and NΔ120 mutant proteins were predominantly localized to the cytoplasm, whereas NΔ150 mutant protein localized to the perinuclear region. Scale bar: 20 μm. (**D**, **E**) An *Alu* retrotransposition assay was performed as described in Figure 1. Crystal violet-stained G418^R colonies were counted to determine the level of *Alu* retrotransposition. The data shown are the mean ± SD of triplicate experiments. Mo, mock; WT, wild-type hA3G; GFP, GFP only. *$P < 0.005$, *t*-test.

doi: 10.1371/journal.pone.0084228.g002

Oligomerized hA3G inhibits retrotransposition

Figure 3

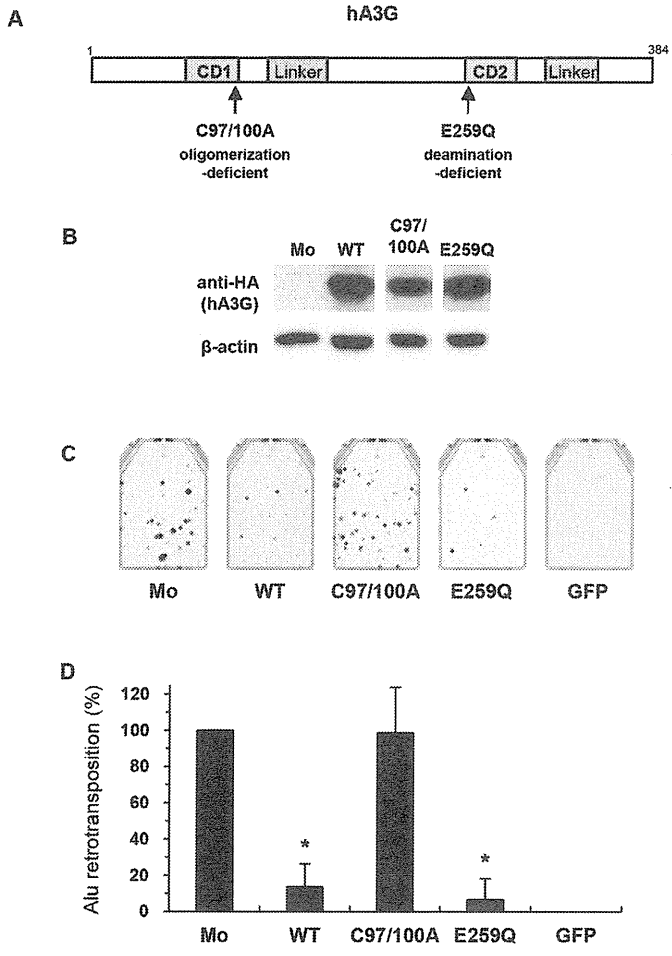

Figure 3. The anti-Alu activity of hA3G is associated with its oligomerization and is independent of its deaminase activity. (**A**) Schematic depiction of two mutants: an oligomerization-deficient mutant, C97/100A, and a deamination-deficient mutant, E259Q. (**B**) Western blot analysis was performed using extracts from 293T cells transfected with plasmids expressing HA-tagged hA3G mutant proteins. Monoclonal antibodies specific for HA (upper) or β-actin (lower) were used. (**C**, **D**) An *Alu* retrotransposition assay was performed as described in Figure 1. A GFP expression vector was used as a negative control. Crystal violet-stained $G418^R$ colonies were counted to determine the level of *Alu* retrotransposition. The data shown are the mean ± SD of triplicate experiments. Mo, mock; WT, wild-type hA3G; GFP, GFP only. $^*P < 0.005$, *t*-test.

doi: 10.1371/journal.pone.0084228.g003

(Y124, Y125, F126, and W127) that have been predicted to be hot spots of protein–protein interaction [68] and have been reported to be critical for the RNA-mediated oligomerization of hA3G [34,59]. The structural model of hA3G-4G(124–127) indicates that the mutant does not form the aromatic cluster, leaving a prominent space between two monomers (compare

Oligomerized hA3G inhibits retrotransposition

Figure 4

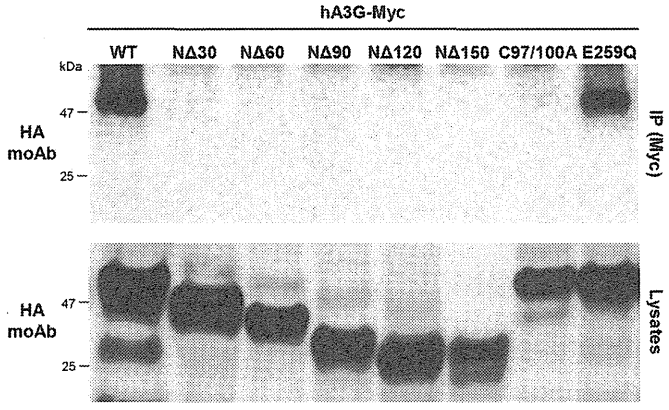

Figure 4. The homooligomerization of hA3G is dependent on the N-terminal 30 amino acid residues of this protein. 293T cells cotransfected with the Myc-tagged and HA-tagged hA3G expression plasmids were immunoprecipitated (IP) with an anti-Myc polyclonal antibody. The resulting complexes were analyzed by immunoblotting with a monoclonal antibody against the HA tag to detect oligomerized hA3G (upper). Cell lysate aliquots were also analyzed in parallel by immunoblotting for the HA tag (lower). WT, wild-type hA3G.

doi: 10.1371/journal.pone.0084228.g004

the left and right panels of Figure 6C and the left and right panels of Figure 6D). Given this result, we then introduced in silico mutations into the five-amino-acid cluster (R24, P25, I26, L27, and S28) of the putative dimer interface (RPILS –> GGGGG; designated 5G(24–28)) (compare the left and right panels of Figure 6E and the left and right panels of Figure 6F). The space between the two monomers of the mutant was clearly comparable to that of 4G(124–127), implying that the 5G(24–28) mutant cannot form a dimer. Based on the structural models, we constructed the myc-tagged N-terminal mutants hA3G-5G(24–28) and hA3G-4G(124–127) to determine whether the former hA3G mutant is unable to physically oligomerize. To assess oligomerization, we performed coimmunoprecipitation-based oligomerization assays using wild-type and mutant hA3G proteins. The 5G(24–28) mutant was not coimmunoprecipitated (Figure 6G), nor was 4G(124–127), suggesting that these mutants do not have the ability to oligomerize. Finally, to determine whether the 4G(124–127) and 5G(24–28) mutants lacks anti-*Alu* activity, we performed the retrotransposition assay and found out that these mutants had completely lost the ability to inhibit *Alu* retrotransposition (Figure 6H). hA3G mutants harboring individual amino acid substitutions (R24G and Y125G) displayed equivalent or moderately less inhibitory activity with comparable dimerization (Figures S3A and S3B). In addition, 5G(24–28) and 4G(124–127) mutations both negatively affect the ability of hA3G to inhibit HIV-1 infection (Figure S4). Taken altogether, these results indicate that the N-terminal amino acid residues 24–28 (RPILS) contribute to the oligomerization of hA3G and its anti-*Alu* retrotransposition activity.

Figure 5

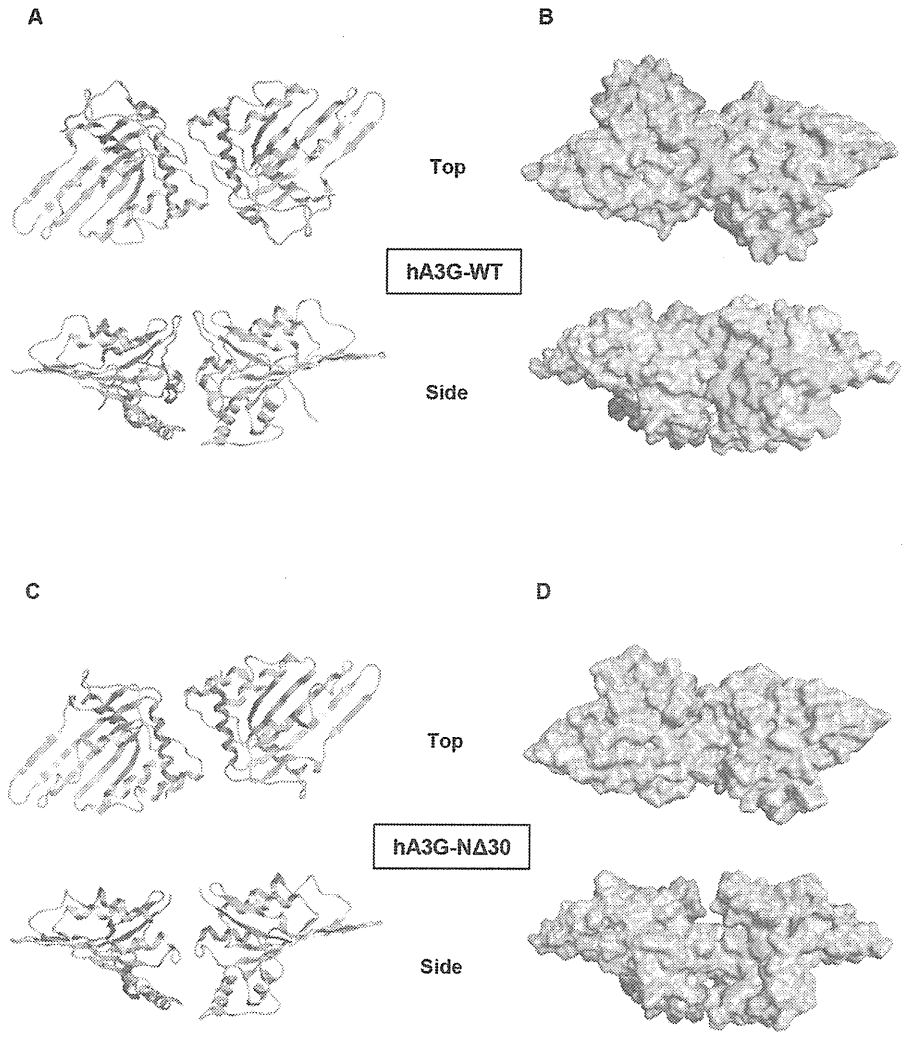

Figure 5. The N-terminal 30 amino acids of hA3G are located at the dimer interface and are therefore key residues for the oligomerization of hA3G. Structural models of the hA3G N-terminal domain. The models were constructed by homology modeling using the X-ray crystal structure of hA2. The head-to-head dimer structure of hA3G N-terminal domain is represented by ribbon models (A and C) and space-filling models (B and D). (**A**, **B**) Views of the top (upper) and side (lower) of wild-type (WT) hA3G. Cyan, N-terminal 30 amino acids of hA3G. (**C**, **D**) Views of the top (upper) and side (lower) of the N-terminal 30-amino-acid deletion mutant of hA3G.

doi: 10.1371/journal.pone.0084228.g005

Oligomerized hA3G inhibits retrotransposition

Figure 6

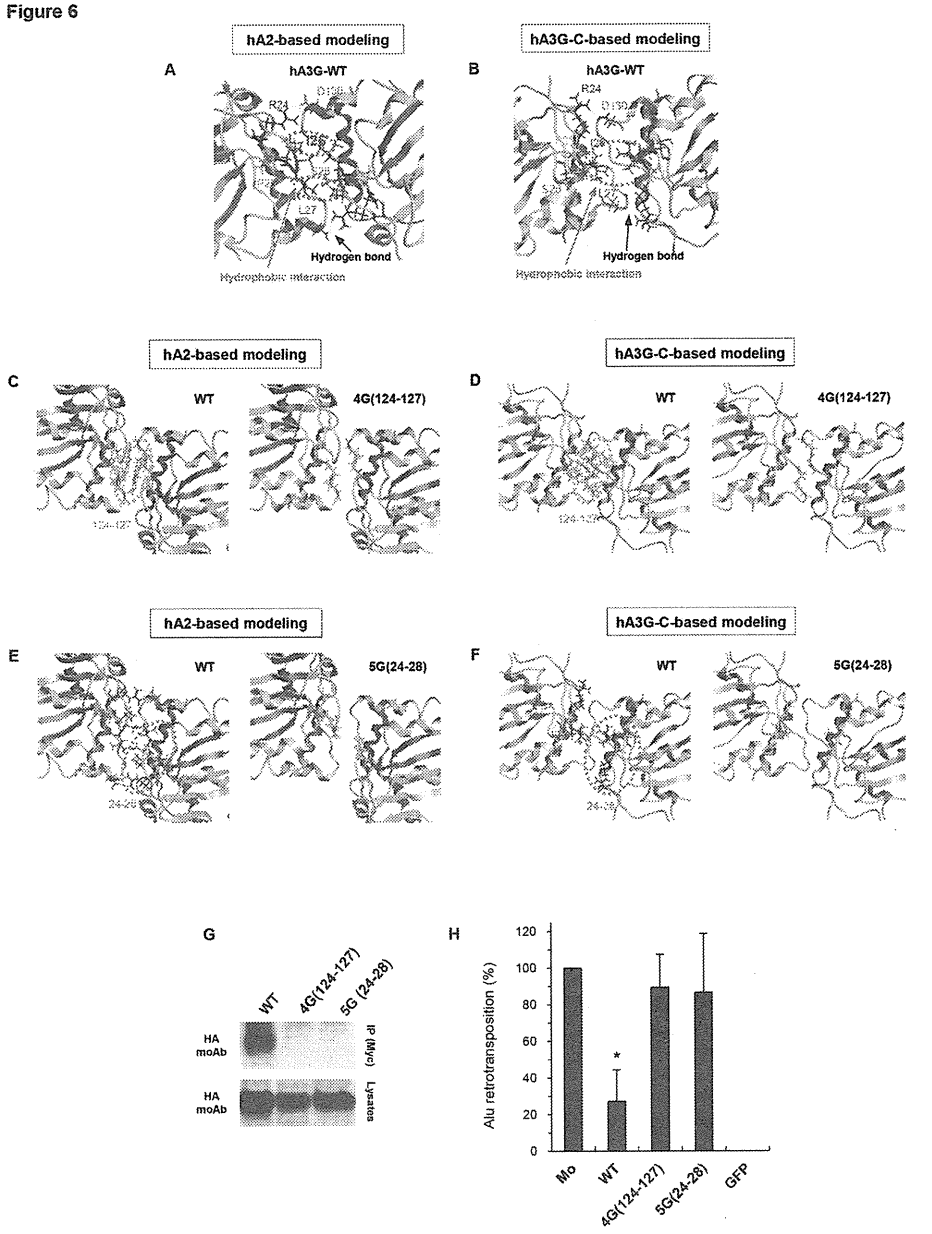

Figure 6. Residues 24–28, as well as known residues 124–127, contribute to the ability of hA3G to homooligomerize and its inhibitory activity against Alu retrotransposition. (A–F) Structural models of hA3G dimer based on the human APOBEC2 (hA2) crystal structure (A, C, and E) and the C-terminal hA3G (hA3G-C) NMR structure (B, D, and F). (**A**, **B**) The interaction surface of the hA3G N-terminal domain in the head-to-head dimer is shown. The hydrophobic interactions formed between either I26 or L27 (green) and their counterpart residues of another monomer (green) are encircled by green dotted lines. A hydrogen bond is formed between a basic residue R24 (blue) and another monomer's D130 (red). Another hydrogen bond is formed between the S28 residues (pink) of two monomers. Structural stability may be conferred by P25 (orange). (**C**, **D**) The dimer interface at amino acid residues 124–127. Left panel, the aromatic amino acid cluster (YYFW) at positions 124–127 is depicted in light green; right panel, the substitution of these residues with glycines is shown in cyan. (**E**, **F**) The dimer interface at amino acid residues 24–28. Left panel, the dimer interface residues (RPILS) at positions 24–28 are depicted in colors similar to those in A; right panel, substitution of these residues with glycines is shown in cyan. (**G**) IP-Western blot analysis was performed as described in Figure 4; upper, IP; lower, cell lysates. (**H**) An *Alu* retrotransposition assay was performed as described in Figure 1. Crystal violet-stained G418R colonies were counted to determine the level of *Alu* retrotransposition. The data shown are the mean ±SD of triplicate experiments. Mo, mock; WT, wild-type hA3G; GFP, GFP only. *P < 0.05, **P < 0.005, t-test.

doi: 10.1371/journal.pone.0084228.g006

hA3G oligomerization is associated with the inhibition of L1 retrotransposition

The inhibitory effects of the hA3G protein on *Alu* retrotransposition resembles its effects on L1 retrotransposition in two regards, first, that hA3G showed similar levels of inhibitory activity against the both retrotransposition events (Figure 1C and ref [37,40]), and second, that the hA3G restriction of retrotransposition is independent of deamination in both cases (Figure 3C and refs. 35,37). These similarities prompted us to determine whether the inhibition of L1 retrotransposition by hA3G requires hA3G oligomerization, as does the inhibition of *Alu* retrotransposition. We performed an L1 retrotransposition assay using all hA3G mutants that we created in this study. As expected, the mutants that do not form oligomers, including NΔ30, NΔ60, NΔ90, NΔ120, NΔ150, C97/100A, 5G(24–28), and 4G(124–127), did not inhibit L1 retrotransposition (Figure 7A, 7B, and 7C), whereas, as observed for *Alu* retrotransposition in Figure 3C, the E259Q deamination mutant had a wild-type level of anti-L1 activity (Figure 7B). Thus, the inhibitory effect of hA3G on *Alu* retrotransposition is associated with hA3G oligomerization but independent of its deaminase activity. We therefore postulate that the inhibitory activities of hA3G against *Alu* and L1 retrotransposition might share common mechanism(s).

Discussion

Our present study demonstrated that hA3 family proteins inhibit *Alu* retrotransposition at differential levels, which are very similar to the levels at which these host proteins block L1 retrotransposition. With respect to hA3G, the N-terminal 30 amino acids are important for the anti-*Alu* activity. The ability of hA3G to inhibit *Alu* retrotransposition was independent of its deaminase activity but associated with its oligomerization activity, as previously reported by Hulme et al. [35] and Bulliard et al. [34], respectively. In agreement with these findings, we found that the N-terminal 30 amino acids that are responsible for counteracting *Alu* retrotransposition are required for the oligomerization of this protein. We used structural modeling to identify the specific residues among the N-terminal 30 amino acids that are responsible for the oligomerization of hA3G. We finally identified amino acid residues 24–28 of hA3G as the contributors of oligomerization.

Importantly, these residues were also critical for the inhibitory activity of L1 retrotransposon, suggesting that this activity might involve the same mechanism as that of *Alu* retrotransposition. This hypothesis makes sense because *Alu* elements do not encode a functional reverse transcriptase or endonuclease, and therefore, they need to hijack the L1-encoded enzymatic machinery for retrotransposition through mechanisms that are currently unclear. It is intriguing to speculate that hA3G might be able to physically block both the *Alu* and L1 retroelements because hA3G is intrinsically an RNA-binding protein that can associate non-specifically with cellular RNAs [48,59,65,69], including those derived from *Alu* retroelements [34,70], or because this protein might directly interact with the L1 ORF2 protein. It is likely that both cases would result in the effective inhibition of *Alu* reverse transcription, and are dependent on the ability of hA3G to form oligomers. In the former case, *Alu* RNA *per se* might help stabilize hA3G oligomer formation, as suggested in Figure S2.

It was somewhat unexpected to find that the N-terminal 30 amino acids of hA3G are required for oligomerization in our study because amino acid positions 124/127 have previously been reported to be important [34,58,59]. Indeed, although only minor effects of either a single R24 or S28 mutation on oligomerization were shown by Huthoff et al. [59] and Bulliard et al. [34] (the former of which was confirmed in Figure S3A), respectively, our study revealed that the previously unappreciated amino acid positions 24–28 among these first 30 residues are responsible for the ability of hA3G to homooligomerize. The dependence of oligomerization on these residues is most likely because not only the amino acids R24 and S28 but also the residues between them are involved in the formation of the interaction interface of an hA3G dimer, as shown in our structural models (Figure 6). This study also reveals that both the amino acid residues 24–28 and 124–127 are equally important for the oligomerization of hA3G. Regarding this point, we assume that the lack or a functional defect of a single interaction interface would be able to totally abolish the protein-protein interaction by leading to the structural destabilization.

Whereas transcriptional repressors such as SRY, SOX2 and methyl-CpG-binding protein 2 have been reported to negatively regulate L1 retrotransposition at the transcriptional levels [71-73], post-transcriptional L1 regulation (apart from that by endogenously encoded small interfering RNAs [74]) like premature polyadenylation and aberrant splicing of its mRNA was also shown to result in a negative influence on L1 expression [75]. In the latter case, retrotransposition-incompetent L1 elements that encode intact ORF2 protein are still able to create DNA double-strand breaks [76] and therefore keep mobilizing *Alu* elements [5,53]. Particularly in such conditions, hA3 proteins would play pivotal roles in the inhibition of *Alu* retrotransposition, putatively through binding to either the ORF2 protein or *Alu* RNA as described above.

It should be noted that the superfamily-1 RNA helicase protein MOV10 (Moloney Leukemia Virus 10; for review, see ref[77].), which is highly conserved across a wide range of species, has recently been reported to inhibit not only infection by several retroviruses, such as HIV-1, simian immunodeficiency virus, murine leukemia virus, and equine infectious anemia virus [78,79], but also the retrotransposition of endogenous retroelements [80-82], exactly as hA3G does. Most importantly, MOV10 was identified to be a protein interacting with hA3G in an RNA-dependent manner [83], suggesting that these two proteins may play mutually supporting roles in restricting exogenous viruses and endogenous retroelements. Further analyses are required to elucidate the precise mechanisms by which hA3 family proteins negatively regulate *Alu* and L1 retrotransposition, possibly in cooperation with other cellular factor(s).

Figure 7

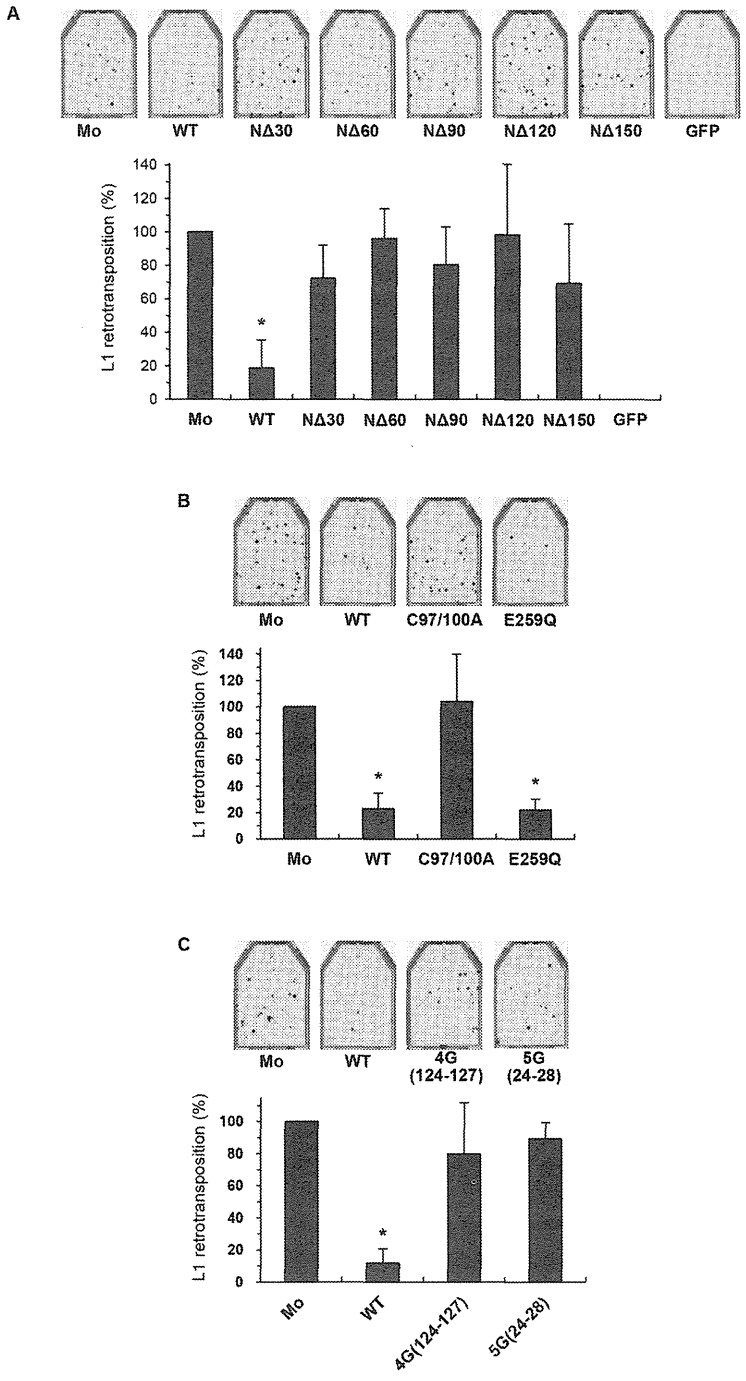

Figure 7. The oligomerization of hA3G is also associated with its anti-L1 activity. HeLa cells were cotransfected with the *neo*^{r}-based L1 expression vector pCEP4/L1mneoI/ColE1 and either a wild-type (WT) or mutant hA3G expression plasmids. Seventy-two hours later, cells were trypsinized, re-seeded into T25 or T75 flasks, and subjected to G418 (1 mg/ml) selection. At 14 days after selection, the resultant G418^R colonies fixed, stained with crystal violet, and counted to determine the level of L1 retrotransposition. (**A**) Compare the results with Figure 2D and 2E. (**B**) Compare the results with Figure 3C and 3D. (**C**) Compare the results with Figure 6H. The data shown are the mean ± SD of triplicate experiments. Mo, mock; WT, wild-type hA3G; GFP, GFP only. *$P < 0.005$, *t*-test.

doi: 10.1371/journal.pone.0084228.g007

Supporting Information

Figure S1. Inhibitory effect of hA3G deletion mutants on HIV-1 infection was evaluated by cotransfecting 293T cells with hA3G and VSV-G plasmids, together with a luciferase-based Vif (-) Env (-) HIV-1 construct, as described by Iwabu et al. (J. Biol. Chem., 285: 35350-8, 2010).
After 48 h, each viral supernatant was harvested. Normalized supernatants were incubated with 293T cells for additional 48 h. Cells were then lysed and subjected to luciferase assay. The data shown are the mean ± SD of triplicate experiments. RLU: relative light units.
(TIF)

Figure S2. Cellular RNA contributes to the stabilization of hA3G's oligomer. HA-tagged hA3G-WT in the immunoprecipitate as described in Figure 4, with or without RNase A treatment.
(TIF)

Figure S3. hA3G mutants with individual amino acid substitutions. (A) Oligomerization assay was performed by IP-Western blot analysis, as described in Figure 4; upper, IP; lower, cell lysates. (B) An *Alu* retrotransposition assay was performed as described in Figure 1. Crystal violet-stained $G418^R$ colonies were counted to determine the level of *Alu* retrotransposition. The data shown are the mean ±SD of triplicate experiments. Mo, mock; WT, wild-type hA3G; GFP, GFP only. $^*P < 0.05$, $^{**}P < 0.005$, *t*-test.
(TIF)

Figure S4. Inhibitory effect of hA3G oligomerization mutant proteins on HIV-1 infection. The assay was performed as described in Figure S1. The data shown are the mean ± SD of triplicate experiments. RLU: relative light units.
(TIF)

Acknowledgements

We thank Astrid M. Roy-Engel, Nicolas Gilbert, and Thierry Heidmann for the generous gifts of expression plasmids.

Author Contributions

Conceived and designed the experiments: KT. Performed the experiments: TK JFA YI MY HF. Analyzed the data: TK JFA YI MY HS HF KT. Wrote the manuscript: KT.

References

1. Lander ES, Linton LM, Birren B, Nusbaum C, Zody MC et al. (2001) Initial sequencing and analysis of the human genome. Nature 409: 860-921. doi:10.1038/35057062. PubMed: 11237011.
2. Hohjoh H, Singer MF (1996) Cytoplasmic ribonucleoprotein complexes containing human LINE-1 protein and RNA. EMBO J 15: 630-639. PubMed: 8599946.
3. Martin SL (1991) Ribonucleoprotein particles with LINE-1 RNA in mouse embryonal carcinoma cells. Mol Cell Biol 11: 4804-4807. PubMed: 1715025.
4. Cost GJ, Feng Q, Jacquier A, Boeke JD (2002) Human L1 element target-primed reverse transcription in vitro. EMBO J 21: 5899-5910. doi: 10.1093/emboj/cdf592. PubMed: 12411507.
5. Dewannieux M, Esnault C, Heidmann T (2003) LINE-mediated retrotransposition of marked Alu sequences. Nat Genet 35: 41-48. doi: 10.1038/ng1223. PubMed: 12897783.
6. Claverie-Martín F, Flores C, Antón-Gamero M, González-Acosta H, García-Nieto V (2005) The Alu insertion in the CLCN5 gene of a patient with Dent's disease leads to exon 11 skipping. J Hum Genet 50: 370-374. doi:10.1007/s10038-005-0265-5. PubMed: 16041495.
7. Li X, Scaringe WA, Hill KA, Roberts S, Mengos A et al. (2001) Frequency of recent retrotransposition events in the human factor IX gene. Hum Mutat 17: 511-519. doi:10.1002/humu.1134. PubMed: 11385709.
8. Meischl C, Boer M, Ahlin A, Roos D (2000) A new exon created by intronic insertion of a rearranged LINE-1 element as the cause of chronic granulomatous disease. Eur J Hum Genet 8: 697-703. doi: 10.1038/sj.ejhg.5200523. PubMed: 10980575.
9. Oldridge M, Zackai EH, McDonald-McGinn DM, Iseki S, Morriss-Kay GM et al. (1999) De novo alu-element insertions in FGFR2 identify a distinct pathological basis for Apert syndrome. Am J Hum Genet 64: 446-461. doi:10.1086/302245. PubMed: 9973282.
10. Yoshida K, Nakamura A, Yazaki M, Ikeda S, Takeda S (1998) Insertional mutation by transposable element, L1, in the DMD gene results in X-linked dilated cardiomyopathy. Hum Mol Genet 7: 1129-1132. doi:10.1093/hmg/7.7.1129. PubMed: 9618170.
11. Narita N, Nishio H, Kitoh Y, Ishikawa Y, Ishikawa Y et al. (1993) Insertion of a 5' truncated L1 element into the 3' end of exon 44 of the dystrophin gene resulted in skipping of the exon during splicing in a case of Duchenne muscular dystrophy. J Clin Invest 91: 1862-1867. doi:10.1172/JCI116402. PubMed: 8387534.
12. Wallace MR, Andersen LB, Saulino AM, Gregory PE, Glover TW et al. (1991) A de novo Alu insertion results in neurofibromatosis type 1. Nature 353: 864-866. doi:10.1038/353864a0. PubMed: 1719426.
13. Kazazian HH Jr., Wong C, Youssoufian H, Scott AF, Phillips DG et al. (1988) Haemophilia A resulting from de novo insertion of L1 sequences represents a novel mechanism for mutation in man. Nature 332: 164-166. doi:10.1038/332164a0. PubMed: 2831458.
14. Baillie JK, Barnett MW, Upton KR, Gerhardt DJ, Richmond TA et al. (2011) Somatic retrotransposition alters the genetic landscape of the human brain. Nature 479: 534-537. doi:10.1038/nature10531. PubMed: 22037309.
15. Coufal NG, Garcia-Perez JL, Peng GE, Yeo GW, Mu Y et al. (2009) L1 retrotransposition in human neural progenitor cells. Nature 460: 1127-1131. doi:10.1038/nature08248. PubMed: 19657334.
16. Economou-Pachnis A, Lohse MA, Furano AV, Tsichlis PN (1985) Insertion of long interspersed repeated elements at the Igh (immunoglobulin heavy chain) and Mlvi-2 (Moloney leukemia virus integration 2) loci of rats. Proc Natl Acad Sci U S A 82: 2857-2861. doi: 10.1073/pnas.82.9.2857. PubMed: 2986141.
17. Morse B, Rotherg PG, South VJ, Spandorfer JM, Astrin SM (1988) Insertional mutagenesis of the myc locus by a LINE-1 sequence in a human breast carcinoma. Nature 333: 87-90. doi:10.1038/333087a0. PubMed: 2834650.
18. Miki Y, Nishisho I, Horii A, Miyoshi Y, Utsunomiya J et al. (1992) Disruption of the APC gene by a retrotransposal insertion of L1 sequence in a colon cancer. Cancer Res 52: 643-645. PubMed: 1310068.
19. Shukla R, Upton Kyle R, Muñoz-Lopez M, Gerhardt Daniel J, Fisher Malcolm E et al. (2013) Endogenous Retrotransposition Activates Oncogenic Pathways in Hepatocellular Carcinoma. Cell 153: 101-111. doi:10.1016/j.cell.2013.02.032. PubMed: 23540693.
20. Sheehy AM, Gaddis NC, Choi JD, Malim MH (2002) Isolation of a human gene that inhibits HIV-1 infection and is suppressed by the viral Vif protein. Nature 418: 646-650. doi:10.1038/nature00939. PubMed: 12167863.
21. Harris RS, Bishop KN, Sheehy AM, Craig HM, Petersen-Mahrt SK et al. (2003) DNA deamination mediates innate immunity to retroviral infection. Cell 113: 803-809. doi:10.1016/S0092-8674(03)00423-9. PubMed: 12809610.
22. Mangeat B, Turelli P, Caron G, Friedli M, Perrin L et al. (2003) Broad antiretroviral defence by human APOBEC3G through lethal editing of

nascent reverse transcripts. Nature 424: 99-103. doi:10.1038/nature01709. PubMed: 12808466.
23. Zhang H, Yang B, Pomerantz RJ, Zhang C, Arunachalam SC et al. (2003) The cytidine deaminase CEM15 induces hypermutation in newly synthesized HIV-1 DNA. Nature 424: 94-98. doi:10.1038/nature01707. PubMed: 12808465.
24. Mariani R, Chen D, Schröfelbauer B, Navarro F, König R et al. (2003) Species-specific exclusion of APOBEC3G from HIV-1 virions by Vif. Cell 114: 21-31. doi:10.1016/S0092-8674(03)00515-4. PubMed: 12859895.
25. Bogerd HP, Doehle BP, Wiegand HL, Cullen BR (2004) A single amino acid difference in the host APOBEC3G protein controls the primate species specificity of HIV type 1 virion infectivity factor. Proc Natl Acad Sci U S A 101: 3770-3774. doi:10.1073/pnas.0307713101. PubMed: 14999100.
26. Mangeat B, Turelli P, Liao S, Trono D (2004) A single amino acid determinant governs the species-specific sensitivity of APOBEC3G to Vif action. J Biol Chem 279: 14481-14483. doi:10.1074/jbc.C400060200. PubMed: 14966139.
27. Schröfelbauer B, Chen D, Landau NR (2004) A single amino acid of APOBEC3G controls its species-specific interaction with virion infectivity factor (Vif). Proc Natl Acad Sci U S A 101: 3927-3932. doi:10.1073/pnas.0307132101. PubMed: 14978281.
28. Russell RA, Wiegand HL, Moore MD, Schäfer A, McClure MO et al. (2005) Foamy virus Bet proteins function as novel inhibitors of the APOBEC3 family of innate antiretroviral defense factors. J Virol 79: 8724-8731. doi:10.1128/JVI.79.14.8724-8731.2005. PubMed: 15994766.
29. Delebecque F, Suspène R, Calattini S, Casartelli N, Saïb A et al. (2006) Restriction of foamy viruses by APOBEC cytidine deaminases. J Virol 80: 605-614. doi:10.1128/JVI.80.2.605-614.2006. PubMed: 16378963.
30. Sasada A, Takaori-Kondo A, Shirakawa K, Kobayashi M, Abudu A et al. (2005) APOBEC3G targets human T-cell leukemia virus type 1. Retrovirology 2: 32. doi:10.1186/1742-4690-2-S1-S32. PubMed: 15943885.
31. Kobayashi M, Takaori-Kondo A, Shindo K, Abudu A, Fukunaga K et al. (2004) APOBEC3G targets specific virus species. J Virol 78: 8238-8244. doi:10.1128/JVI.78.15.8238-8244.2004. PubMed: 15254195.
32. Okeoma CM, Lovsin N, Peterlin BM, Ross SR (2007) APOBEC3 inhibits mouse mammary tumour virus replication in vivo. Nature 445: 927-930. doi:10.1038/nature05540. PubMed: 17259974.
33. Esnault C, Heidmann O, Delebecque F, Dewannieux M, Ribet D et al. (2005) APOBEC3G cytidine deaminase inhibits retrotransposition of endogenous retroviruses. Nature 433: 430-433. doi:10.1038/nature03238. PubMed: 15674295.
34. Bulliard Y, Turelli P, Röhrig UF, Zoete V, Mangeat B et al. (2009) Functional analysis and structural modeling of human APOBEC3G reveal the role of evolutionarily conserved elements in the inhibition of human immunodeficiency virus type 1 infection and Alu transposition. J Virol 83: 12611-12621. doi:10.1128/JVI.01491-09. PubMed: 19776130.
35. Hulme AE, Bogerd HP, Cullen BR, Moran JV (2007) Selective inhibition of Alu retrotransposition by APOBEC3G. Gene 390: 199-205. doi:10.1016/j.gene.2006.08.032. PubMed: 17079095.
36. Chiu YL, Witkowska HE, Hall SC, Santiago M, Soros VB et al. (2006) High-molecular-mass APOBEC3G complexes restrict Alu retrotransposition. Proc Natl Acad Sci U S A 103: 15588-15593. doi:10.1073/pnas.0604524103. PubMed: 17030807.
37. Kinomoto M, Kanno T, Shimura M, Ishizaka Y, Kojima A et al. (2007) All APOBEC3 family proteins differentially inhibit LINE-1 retrotransposition. Nucleic Acids Res 35: 2955-2964. doi:10.1093/nar/gkm181. PubMed: 17439959.
38. Ikeda T, Abd El Galil KH, Tokunaga K, Maeda K, Sata T et al. (2011) Intrinsic restriction activity by apolipoprotein B mRNA editing enzyme APOBEC1 against the mobility of autonomous retrotransposons. Nucleic Acids Res 39: 5538-5554. doi:10.1093/nar/gkr124. PubMed: 21398638.
39. Khatua AK, Taylor HE, Hildreth JE, Popik W (2010) Inhibition of LINE-1 and Alu retrotransposition by exosomes encapsidating APOBEC3G and APOBEC3F. Virology 400: 68-75. doi:10.1016/j.virol.2010.01.021. PubMed: 20153011.
40. Niewiadomska AM, Tian C, Tan L, Wang T, Sarkis PTN et al. (2007) Differential Inhibition of Long Interspersed Element 1 by APOBEC3 Does Not Correlate with High-Molecular-Mass-Complex Formation or P-Body Association. J Virol 81: 9577-9583. doi:10.1128/JVI.02800-06. PubMed: 17582006.
41. Arias JF, Koyama T, Kinomoto M, Tokunaga K (2012) Retroelements versus APOBEC3 family members: No great escape from the magnificent seven. Front Microbiol 3: 275. PubMed: 22912627.
42. Turelli P, Mangeat B, Jost S, Vianin S, Trono D (2004) Inhibition of hepatitis B virus replication by APOBEC3G. Science 303: 1829. doi:10.1126/science.1092066. PubMed: 15031497.
43. Noguchi C, Ishino H, Tsuge M, Fujimoto Y, Imamura M et al. (2005) G to A hypermutation of hepatitis B virus. Hepatology 41: 626-633. doi:10.1002/hep.20580. PubMed: 15726649.
44. OhAinle M, Kerns JA, Malik HS, Emerman M (2006) Adaptive evolution and antiviral activity of the conserved mammalian cytidine deaminase APOBEC3H. J Virol 80: 3853-3862. doi:10.1128/JVI.80.8.3853-3862.2006. PubMed: 16571802.
45. Sawyer SL, Emerman M, Malik HS (2004) Ancient adaptive evolution of the primate antiviral DNA-editing enzyme APOBEC3G. PLoS Biol 2: E275. doi:10.1371/journal.pbio.0020275. PubMed: 15269786.
46. Schumann GG (2007) APOBEC3 proteins: major players in intracellular defence against LINE-1-mediated retrotransposition. Biochem Soc Trans 35: 637-642. doi:10.1042/BST0350637. PubMed: 17511669.
47. Stenglein MD, Harris RS (2006) APOBEC3B and APOBEC3F inhibit L1 retrotransposition by a DNA deamination-independent mechanism. J Biol Chem 281: 16837-16841. doi:10.1074/jbc.M602367200. PubMed: 16648136.
48. Muckenfuss H, Hamdorf M, Held U, Perkovic M, Löwer J et al. (2006) APOBEC3 proteins inhibit human LINE-1 retrotransposition. J Biol Chem 281: 22161-22172. doi:10.1074/jbc.M601716200. PubMed: 16735504.
49. Bogerd HP, Wiegand HL, Hulme AE, Garcia-Perez JL, O'Shea KS et al. (2006) Cellular inhibitors of long interspersed element 1 and Alu retrotransposition. Proc Natl Acad Sci U S A 103: 8780-8785. doi:10.1073/pnas.0603313103. PubMed: 16728505.
50. Turelli P, Vianin S, Trono D (2004) The innate antiretroviral factor APOBEC3G does not affect human LINE-1 retrotransposition in a cell culture assay. J Biol Chem 279: 43371-43373. doi:10.1074/jbc.C400334200. PubMed: 15322092.
51. Tan L, Sarkis PT, Wang T, Tian C, Yu XF (2009) Sole copy of Z2-type human cytidine deaminase APOBEC3H has inhibitory activity against retrotransposons and HIV-1. FASEB J 23: 279-287. doi:10.1096/fj.07-088781. PubMed: 18827027.
52. Gilbert N, Lutz-Prigge S, Moran JV (2002) Genomic deletions created upon LINE-1 retrotransposition. Cell 110: 315-325. doi:10.1016/S0092-8674(02)00828-0. PubMed: 12176319.
53. Wallace N, Wagstaff BJ, Deininger PL, Roy-Engel AM (2008) LINE-1 ORF1 protein enhances Alu SINE retrotransposition. Gene 419: 1-6. doi:10.1016/j.gene.2008.04.007. PubMed: 18534786.
54. Iwabu Y, Fujita H, Kinomoto M, Kaneko K, Ishizaka Y et al. (2009) HIV-1 accessory protein Vpu internalizes cell-surface BST-2/tetherin through transmembrane interactions leading to lysosomes. J Biol Chem 284: 35060-35072. doi:10.1074/jbc.M109.058305. PubMed: 19837671.
55. Iwabu Y, Kinomoto M, Tatsumi M, Fujita H, Shimura M et al. (2010) Differential anti-APOBEC3G activity of HIV-1 Vif proteins derived from different subtypes. J Biol Chem 285: 35350-35358. doi:10.1074/jbc.M110.173286. PubMed: 20833716.
56. Prochnow C, Bransteitter R, Klein MG, Goodman MF, Chen XS (2007) The APOBEC-2 crystal structure and functional implications for the deaminase AID. Nature 445: 447-451. doi:10.1038/nature05492. PubMed: 17187054.
57. Chen KM, Harjes E, Gross PJ, Fahmy A, Lu Y et al. (2008) Structure of the DNA deaminase domain of the HIV-1 restriction factor APOBEC3G. Nature 452: 116-119. doi:10.1038/nature06638. PubMed: 18288108.
58. Lavens D, Peelman F, Van der Heyden J, Uyttendaele I, Catteeuw D et al. (2010) Definition of the interacting interfaces of Apobec3G and HIV-1 Vif using MAPPIT mutagenesis analysis. Nucleic Acids Res 38: 1902-1912. doi:10.1093/nar/gkp1154. PubMed: 20015971.
59. Huthoff H, Autore F, Gallois-Montbrun S, Fraternali F, Malim MH (2009) RNA-dependent oligomerization of APOBEC3G is required for restriction of HIV-1. PLoS Pathog 5: e1000330. PubMed: 19266078.
60. Zhang K-L, Mangeat B, Ortiz M, Zoete V, Trono D et al. (2007) Model Structure of Human APOBEC3G. PLOS ONE 2: e378. doi:10.1371/journal.pone.0000378. PubMed: 17440614.
61. Shirakawa K, Takaori-Kondo A, Yokoyama M, Izumi T, Matsui M et al. (2008) Phosphorylation of APOBEC3G by protein kinase A regulates its interaction with HIV-1 Vif. Nat Struct Mol Biol 15: 1184-1191. doi:10.1038/nsmb.1497. PubMed: 18836454.
62. Labute P (2008) The generalized Born/volume integral implicit solvent model: estimation of the free energy of hydration using London dispersion instead of atomic surface area. J Comput Chem 29: 1693-1698. doi:10.1002/jcc.20933. PubMed: 18307169.

63. Ponder JW, Case DA (2003) Force fields for protein simulations. Adv Protein Chem 66: 27-85. doi:10.1016/S0065-3233(03)66002-X. PubMed: 14631816.
64. Onufriev A, Bashford D, Case DA (2000) Modification of the Generalized Born Model Suitable for Macromolecules. Journal of Physical Chemistry B 104: 3712-3720. doi:10.1021/jp993855a.
65. Navarro F, Bollman B, Chen H, König R, Yu Q et al. (2005) Complementary function of the two catalytic domains of APOBEC3G. Virology 333: 374-386. doi:10.1016/j.virol.2005.01.011. PubMed: 15721369.
66. Newman EN, Holmes RK, Craig HM, Klein KC, Lingappa JR et al. (2005) Antiviral function of APOBEC3G can be dissociated from cytidine deaminase activity. Curr Biol 15: 166-170. doi:10.1016/j.cub.2004.12.068. PubMed: 15668174.
67. Shandilya SM, Nalam MN, Nalivaika EA, Gross PJ, Valesano JC et al. (2010) Crystal structure of the APOBEC3G catalytic domain reveals potential oligomerization interfaces. Structure 18: 28-38. doi:10.1016/j.str.2009.10.016. PubMed: 20152150.
68. Cho K-i, Kim D, Lee D (2009) A feature-based approach to modeling protein–protein interaction hot spots. Nucleic Acids Res 37: 2672-2687. doi:10.1093/nar/gkp132. PubMed: 19273533.
69. Iwatani Y, Chan DS, Wang F, Maynard KS, Sugiura W et al. (2007) Deaminase-independent inhibition of HIV-1 reverse transcription by APOBEC3G. Nucleic Acids Res 35: 7096-7108. doi:10.1093/nar/gkm750. PubMed: 17942420.
70. Bach D, Peddi S, Mangeat B, Lakkaraju A, Strub K et al. (2008) Characterization of APOBEC3G binding to 7SL RNA. Retrovirology 5: 54. doi:10.1186/1742-4690-5-54. PubMed: 18597676.
71. Muotri AR, Marchetto MC, Coufal NG, Oefner R, Yeo G et al. (2010) L1 retrotransposition in neurons is modulated by MeCP2. Nature 468: 443-446. doi:10.1038/nature09544. PubMed: 21085180.
72. Muotri AR, Chu VT, Marchetto MCN, Deng W, Moran JV et al. (2005) Somatic mosaicism in neuronal precursor cells mediated by L1 retrotransposition. Nature 435: 903-910. doi:10.1038/nature03663. PubMed: 15959507.
73. Tchénio T, Casella JF, Heidmann T (2000) Members of the SRY family regulate the human LINE retrotransposons. Nucleic Acids Res 28: 411-415. doi:10.1093/nar/28.2.411. PubMed: 10606637.
74. Yang N, Kazazian HH Jr. (2006) L1 retrotransposition is suppressed by endogenously encoded small interfering RNAs in human cultured cells. Nat Struct Mol Biol 13: 763-771. doi:10.1038/nsmb1141. PubMed: 16936727.
75. Belancio VP, Roy-Engel AM, Pochampally RR, Deininger P (2010) Somatic expression of LINE-1 elements in human tissues. Nucleic Acids Res 38: 3909-3922. doi:10.1093/nar/gkq132. PubMed: 20215437.
76. Gasior SL, Wakeman TP, Xu B, Deininger PL (2006) The human LINE-1 retrotransposon creates DNA double-strand breaks. J Mol Biol 357: 1383-1393. doi:10.1016/j.jmb.2006.01.089. PubMed: 16490214.
77. Zheng YH, Jeang KT, Tokunaga K (2012) Host restriction factors in retroviral infection: promises in virus-host interaction. Retrovirology 9: 112. doi:10.1186/1742-4690-9-S2-P112. PubMed: 23254112.
78. Wang X, Han Y, Dang Y, Fu W, Zhou T et al. (2010) Moloney leukemia virus 10 (MOV10) protein inhibits retrovirus replication. J Biol Chem 285: 14346-14355. doi:10.1074/jbc.M110.109314. PubMed: 20215113.
79. Furtak V, Mulky A, Rawlings SA, Kozhaya L, Lee K et al. (2010) Perturbation of the P-body component Mov10 inhibits HIV-1 infectivity. PLOS ONE 5: e9081. doi:10.1371/journal.pone.0009081. PubMed: 20140200.
80. Lu C, Luo Z, Jäger S, Krogan NJ, Peterlin BM (2012) Moloney leukemia virus type 10 inhibits reverse transcription and retrotransposition of intracisternal a particles. J Virol 86: 10517-10523. doi:10.1128/JVI.00868-12. PubMed: 22811528.
81. Goodier JL, Cheung LE, Kazazian HH Jr. (2012) MOV10 RNA helicase is a potent inhibitor of retrotransposition in cells. PLoS Genet 8: e1002941. PubMed: 23093941.
82. Arjan-Odedra S, Swanson CM, Sherer NM, Wolinsky SM, Malim MH (2012) Endogenous MOV10 inhibits the retrotransposition of endogenous retroelements but not the replication of exogenous retroviruses. Retrovirology 9: 53. doi:10.1186/1742-4690-9-53. PubMed: 22727223.
83. Gallois-Montbrun S, Kramer B, Swanson CM, Byers H, Lynham S et al. (2007) Antiviral protein APOBEC3G localizes to ribonucleoprotein complexes found in P bodies and stress granules. J Virol 81: 2165-2178. doi:10.1128/JVI.02287-06. PubMed: 17166910.

JVI
Journals.ASM.org

Generation of Rhesus Macaque-Tropic HIV-1 Clones That Are Resistant to Major Anti-HIV-1 Restriction Factors

Masako Nomaguchi,[a] Masaru Yokoyama,[b] Ken Kono,[c] Emi E. Nakayama,[c] Tatsuo Shioda,[c] Naoya Doi,[a,d] Sachi Fujiwara,[a] Akatsuki Saito,[d,e] Hirofumi Akari,[e] Kei Miyakawa,[d,f] Akihide Ryo,[f] Hirotaka Ode,[d,g] Yasumasa Iwatani,[g] Tomoyuki Miura,[h] Tatsuhiko Igarashi,[h] Hironori Sato,[b] Akio Adachi[a]

Department of Microbiology, Institute of Health Biosciences, The University of Tokushima Graduate School, Tokushima, Tokushima, Japan[a]; Laboratory of Viral Genomics, Pathogen Genomics Center, National Institute of Infectious Diseases, Musashimurayama, Tokyo, Japan[b]; Department of Viral Infections, Research Institute for Microbial Diseases, Osaka University, Suita, Osaka, Japan[c]; Japanese Foundation for AIDS Prevention, Chiyoda-ku, Tokyo, Japan[d]; Section of Comparative Immunology and Microbiology, Center for Human Evolution Modeling Research, Primate Research Institute, Kyoto University, Inuyama, Aichi, Japan[e]; Department of Microbiology, Yokohama City University School of Medicine, Yokohama, Kanagawa, Japan[f]; Clinical Research Center, Department of Infectious Diseases and Immunology, National Hospital Organization Nagoya Medical Center, Nagoya, Aichi, Japan[g]; Laboratory of Primate Model, Experimental Research Center for Infectious Diseases, Institute for Virus Research, Kyoto University, Kyoto, Kyoto, Japan[h]

Human immunodeficiency virus type 1 (HIV-1) replication in macaque cells is restricted mainly by antiviral cellular APOBEC3, TRIM5α/TRIM5CypA, and tetherin proteins. For basic and clinical HIV-1/AIDS studies, efforts to construct macaque-tropic HIV-1 (HIV-1mt) have been made by us and others. Although rhesus macaques are commonly and successfully used as infection models, no HIV-1 derivatives suitable for *in vivo* rhesus research are available to date. In this study, to obtain novel HIV-1mt clones that are resistant to major restriction factors, we altered Gag and Vpu of our best HIV-1mt clone described previously. First, by sequence- and structure-guided mutagenesis, three amino acid residues in Gag-capsid (CA) (M94L/R98S/G114Q) were found to be responsible for viral growth enhancement in a macaque cell line. Results of *in vitro* TRIM5α susceptibility testing of HIV-1mt carrying these substitutions correlated well with the increased viral replication potential in macaque peripheral blood mononuclear cells (PBMCs) with different *TRIM5* alleles, suggesting that the three amino acids in HIV-1mt CA are involved in the interaction with TRIM5α. Second, we replaced the transmembrane domain of Vpu of this clone with the corresponding region of simian immunodeficiency virus SIVgsn166 Vpu. The resultant clone, MN4/LSDQgtu, was able to antagonize macaque but not human tetherin, and its Vpu effectively functioned during viral replication in a macaque cell line. Notably, MN4/LSDQgtu grew comparably to SIVmac239 and much better than any of our other HIV-1mt clones in rhesus macaque PBMCs. In sum, MN4/LSDQgtu is the first HIV-1 derivative that exhibits resistance to the major restriction factors in rhesus macaque cells.

Human immunodeficiency virus type 1 (HIV-1) has spread globally in human populations following cross-species transmission of simian immunodeficiency virus (SIV) from chimpanzees (1, 2). HIV-1 replicates well in humans and causes disease-inducing persistent infection only in humans. HIV-1 infection is impeded after virus entry in rhesus macaques (RhMs) and cynomolgus macaques (CyMs), which are frequently used for experimental viral infection studies (3). The block of HIV-1 infection in macaque cells is attributable to intrinsic restriction factors, including APOBEC3, TRIM5α/TRIM5CypA, and tetherin proteins (1, 4–6). These factors exert their antiretroviral activity in a species-specific manner, and HIV-1 effectively subverts their counterparts in human cells (1, 4–6). In contrast, a standard pathogenic clone, SIVmac239, for AIDS model studies evades the restriction factors and replicates well in macaques. HIV-1 and SIVmac239 are mutually related primate lentiviruses and cause AIDS in their respective hosts. Nevertheless, there are significant differences between the two viruses in genome organization, the viral replication profile *in vivo*, and disease progression (7–9). It is therefore most preferable to generate pathogenic HIV-1 derivatives to establish AIDS macaque models (7–9). Importantly, construction of HIV-1 derivatives that overcome the species barrier would contribute much to the understanding of the molecular interaction of viral and host proteins.

Of the intrinsic restriction factors in macaque cells, major determinants of the HIV-1 host range are the APOBEC3 and TRIM5 proteins (4, 8, 10). APOBEC3G is the strongest inhibitor of HIV-1 replication among APOBEC3 family proteins. It exhibits cytidine deaminase activity and causes hypermutation in the HIV-1 genome following incorporation into progeny virions in producer cells. HIV-1 Vif is able to degrade human APOBEC3G and neutralize its antiviral activity but is not effective against macaque APOBEC3G (4–6, 11, 12). Macaque TRIM5 proteins recognize and interact with the incoming HIV-1 cores and inhibit viral infection prior to reverse transcription (4, 6, 13, 14). TRIM5 proteins are composed of N-terminal RING, B-box 2, and coiled-coil domains. The C termini of TRIM5α and TRIM5CypA are the B30.2/SPRY and cyclophilin A (CypA) domains, respectively. All these domains in TRIM5 proteins are necessary to exert full restriction activity. Although the mechanism underlying TRIM5-mediated restriction has not been completely defined, inhibition of viral infection is initiated by capsid (CA) recognition with the

Received 7 June 2013 Accepted 9 August 2013
Published ahead of print 21 August 2013
Address correspondence to Hironori Sato, hirosato@nih.go.jp, or Akio Adachi, adachi@basic.med.tokushima-u.ac.jp.
M.N. and M.Y. contributed equally to this article.

doi:10.1128/JVI.01549-13

B30.2/SPRY or CypA domain. Sequence variation in the two domains determines species-specific restriction of retroviral infection. RhM *TRIM5* genes have been reported to be highly polymorphic (4, 6, 13, 14). Tetherin works as a virion release inhibition factor, and HIV-1 Vpu counteracts human but not macaque tetherin (4–6, 15). Tetherin may not be a potent barrier to limit cross-species transmission relative to APOBEC3G and TRIM5 proteins. However, tetherin antagonism is important for viral replication *in vivo*, because most primate lentiviruses have the ability to counteract tetherin, and tetherin-mediated restriction contributes to inhibiting viral replication *in vivo* (4, 5, 15). Recently, a novel anti-HIV-1 factor, SAMHD1, has been identified (4–6). Several Vpx and Vpr proteins appear to degrade SAMHD1 in a species-specific manner. However, SAMHD1 may be a weak species barrier, since HIV-1 has spread successfully and continuously in humans despite the lack of anti-SAMHD1 activity (4).

We and others have reported the construction of HIV-1 derivatives that have the ability to evade restriction factors for macaque model studies (16–21). As a common feature, all reported macaque-tropic HIV-1 (HIV-1mt) clones have the *vif* gene, which can neutralize macaque APOBEC3G (e.g., SIVmac239 *vif*). This modification is essential to evade APOBEC3G restriction and to gain the ability to replicate in macaque cells. To circumvent the restriction by TRIM5 proteins, two approaches have been taken. One approach is the use of pig-tailed macaques that do not express HIV-1-restrictive TRIM5 proteins. In this case, HIV-1 derivatives carrying authentic HIV-1 CA have been used as challenge viruses (stHIV-1_{SV} [16] and HSIV-vif [21]). Another approach is the replacement of the entire HIV-1 CA with the corresponding region of SIVmac239 (stHIV-1_{SCA+SV} [16, 17]). Although stHIV-1_{SCA+SV} replicates well in RhM cells, the CA region is not derived from HIV-1. Recently, chimeric viruses between simian-human immunodeficiency virus ($SHIV_{DH12}$ and $SHIV_{AD8}$) and an HIV-1 derivative (stHIV-1gsnU) that display anti-macaque tetherin activity have been reported (22, 23). However, the former construct is SHIV, and the latter is pig-tailed macaque-tropic HIV-1 carrying full-length SIVgsn71 (SIV from greater spot-nosed monkey) Vpu. While RhMs have been commonly and frequently used for viral infection experiments, no RhM-tropic HIV-1 derivatives that exhibit resistance to known major intrinsic restriction factors (APOBEC3, TRIM5, and tetherin proteins) have been reported.

We have previously described a unique HIV-1mt clone, designated MN4Rh-3, which can evade APOBEC3 and TRIM5CypA proteins but not TRIM5α and tetherin restrictions in macaque cells (Fig. 1) (19, 24). In this study, we generated new HIV-1mt clones from MN4Rh-3 that potentially possess an improved capacity to antagonize RhM TRIM5α and tetherin proteins. First, we constructed a number of MN4Rh-3 CA mutant clones; examined their growth potentials in an RhM lymphocyte cell line, M1.3S (25); and selected a new HIV-1mt clone, MN4/LSDQ, carrying only three amino acid substitutions in MN4Rh-3 CA (Fig. 1). MN4/LSDQ exhibited enhanced growth potential accompanied by increased resistance to macaque TRIM5α restriction. Next, we replaced the transmembrane (TM) domain of MN4/LSDQ Vpu with the corresponding region of SIVgsn166 (another SIVgsn) Vpu, which shows anti-macaque tetherin activity (26). The resultant clone, MN4/LSDQgtu, gained the ability to antagonize specifically macaque tetherin (Fig. 1). The replication efficiency of MN4/LSDQgtu in RhM peripheral blood mononuclear cells (PBMCs) was comparable to that of SIVmac239 and was superior to those of the other HIV-1mt clones (MN4Rh-3 and MN4/LSDQ). MN4/LSDQgtu is the first HIV-1 derivative that is highly resistant to the known major restriction factors (APOBEC3, TRIM5, and tetherin proteins) in RhM cells. Generation of MN4/LSDQgtu also served to find amino acid residues in CA involved in the interaction with macaque TRIM5α and to verify HIV-1mt growth enhancement in macaque cells by macaque tetherin antagonism.

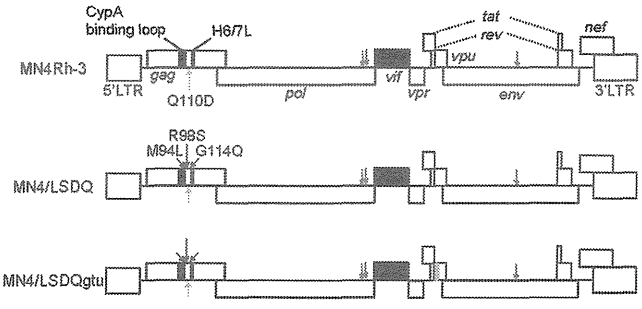

FIG 1 Proviral genome structures of various HIV-1mt clones. HIV-1 NL4-3 (32), SIVmac239 MA239 (71), and SIVgsn166 (GenBank accession number AF468659) sequences are indicated by white, black, and red areas, respectively. Green arrows show adaptive mutations that enhance viral growth potential (47). Orange arrows show the CA-Q110D mutation that augments viral growth in macaque cells/monkeys (19, 24). Blue arrows indicate CA substitutions (M94L/R98S/G114Q) identified in this study that are responsible for viral growth enhancement. H6/7L, loop between helices 6 and 7 in Gag-CA.

MATERIALS AND METHODS

Cells. An RhM lymphocyte cell line, M1.3S (25), was maintained in RPMI 1640 medium containing 10% heat-inactivated fetal bovine serum (FBS) and 50 units/ml of recombinant human interleukin-2 (IL-2) (Bio-Rad Laboratories Inc., Hercules, CA). The human monolayer cell lines 293T (27) and HEp2 (ATCC CCL-23) and the RhM kidney cell line LLC-MK2 (ATCC CCL-7) were maintained in Eagle's minimal essential medium (MEM) containing 10% FBS. MAGI cells (28) were cultured in MEM containing 10% FBS, 200 μg/ml G418 (Sigma-Aldrich Co., St. Louis, MO), and 100 μg/ml hygromycin B (Sigma-Aldrich Co.).

Plasmid DNA. The construction of MN4Rh-3, SIVmac239 clone MA239N, and its *nef*-deficient variant MA239N-ΔN was described previously (19, 25). CA alterations of HIV-1mt proviral clones were performed by replacing target sites of HIV-1mt CA with the corresponding sites of SIVmac239 (both codons and amino acids were changed to those of SIVmac239) by using the QuikChange site-directed mutagenesis kit (Agilent Technologies Inc., Santa Clara, CA). MN4/LSDQ was generated by introducing the following codon/amino acid substitutions into MN4Rh-3 (uppercase letters represent amino acids and lowercase letters represent codons): M(atg) to L(ctt) at amino acid position 94, R(agg) to S(tca) at position 98, and G(gga) to Q(cag) at position 114. Each *vpu* gene of SIVmon (SIV from mona monkey)/SIVmus (SIV from mustached monkey)/SIVgsn (SIVmon/mus/gsn) was synthesized (TaKaRa Bio Inc., Otsu, Japan) and cloned into pSG-cFLAG to express mon-, mus-, and gsn-Vpu, respectively, as described previously (29). Full-length Vpu sequences composed of the TM domain of SIVmon/mus/gsn Vpu and the cytoplasmic domain of HIV-1_{NL4-3} Vpu (monTM-, musTM-, and gsnTM-Vpu, respectively) were made by overlapping PCR and inserted into the pSG-cFLAG expression vector, as described previously (29). The resultant clones were designated pSG-VpucFLAG constructs. RhM and human tetherin sequences were amplified by PCR using cDNAs from M1.3S cells and HeLa cells, respectively. The amplified products were cloned into the pCIneo vector (Promega Corporation, Madison, WI) to generate pCIneo-RhM tetherin and pCIneo-Human tetherin. The sequence of RhM tetherin from M1.3S cells was identical to that of an RhM

tetherin variant [Mac(m)3] (30, 31). For flow cytometry analysis, pIRES-HIV-1-Vpu-hrGFP and pIRES-gsnTM-Vpu-hrGFP were constructed as described previously (29). The MN4/LSDQdtu clone was constructed by replacing the TM domain of MN4/LSDQ Vpu with the corresponding region of HIV-1_{DH12} Vpu (22) by using the QuikChange site-directed mutagenesis kit (Agilent Technologies Inc.). The MN4/LSDQgtu clone was generated by overlapping PCR between MN4/LSDQ and gsnTM-Vpu. *vpu*-deficient HIV-1mt clones were constructed by changing the initiation codon (ATG) to AGG and the second codon of each construct to TAG (stop codon).

Virus stocks and reverse transcriptase assay. Virus stocks were prepared from 293T cells transfected with proviral clones by the calcium-phosphate coprecipitation method (32). Virion-associated reverse transcriptase (RT) activity was measured as described previously (33), with the following modifications: 5 μl of culture supernatant was mixed with 25 μl of an RT reaction mixture containing a template primer of poly(A) (500 μg/ml; Midland Certified Reagent Company Inc., Midland, TX) and oligo$(dT)_{12-18}$ (1.25 μg/ml; New England BioLabs Inc., Ipswich, MA) in 50 mM Tris (pH 7.8), 75 mM KCl, 2 mM dithiothreitol, 5 mM $MgCl_2$, 0.05% Nonidet P-40, and 9.25 kBq of [α-^{32}P]dTTP (29.6 TBq/mmol; Perkin-Elmer Inc., Waltham, MA). After incubation at 37°C for 3 h, 10 μl of the reaction mixture was spotted onto DE81 anion-exchange paper (GE Healthcare UK Ltd., Buckinghamshire, England) and washed four times with 2× SSC (0.3 M NaCl plus 0.03 M sodium citrate) to remove unincorporated [α-^{32}P]dTTP. Spots were then counted with a scintillation counter.

Virus replication assays. Virus replication in M1.3S cells was monitored as described previously (25). For infection of macaque primary cells, RhM and CyM PBMCs were separated by Ficoll-Paque Plus (GE Healthcare UK Ltd.) and stimulated with RPMI 1640 medium containing 10% FBS, 50 units/ml of recombinant human IL-2, and 2 μg/ml of phytohemagglutinin L (PHA-L) (Roche Diagnostics GmbH, Mannheim, Germany). Primary PBMCs without $CD8^+$ cell depletion were used in this study. On day 3 poststimulation, cells were spin infected (34) with equal amounts of viruses prepared from transfected 293T cells and cultured in the presence of IL-2. Viral growth was monitored by RT activity released into the culture supernatants. The genotype of *TRIM5* alleles was analyzed as described previously (35).

TRIM5α susceptibility assays. Assays using recombinant Sendai virus (SeV)-RhM TRIM5α and SeV-CyM TRIM5α expression systems were performed as described previously (36). MT4 cells (10^5) were infected with SeV expressing each TRIM5α at a multiplicity of infection of 10 PFU per cell and incubated at 37°C for 9 h. Cells were then superinfected with HIV-1mt derivatives (20 ng of Gag-p24) or SIVmac239 (20 ng of Gag-p27). Culture supernatants were collected at intervals, and the amount of Gag-p24 or Gag-p27 produced was determined by using RETROtek antigen enzyme-linked immunosorbent assay (ELISA) kits (ZeptoMetrix Corporation, Buffalo, NY).

Virion release assays. Tetherin-null 293T cells were used for virion release assays. For analysis of Vpu expression vectors, subconfluent 293T cells in 24-well dishes were cotransfected with *vpu*-deficient MN4Rh-3 (300 ng), pCIneo-RhM tetherin (5 ng), and various pSG-VpucFLAG vectors (200 ng) by using Lipofectamine 2000 (Life Technologies Corporation, Carlsbad, CA). On day 2 posttransfection, virion production in the cell culture supernatants was measured by RT assays. For analysis of proviral clones, 700 ng of MA239N/MA239N-ΔN or 300 ng of MN4 derivatives and an appropriate amount of pCIneo-RhM tetherin or pCIneo-Human tetherin were used for cotransfection.

Flow cytometry analysis. Flow cytometry analysis was performed to examine cell surface CD4 or tetherin downregulation by Vpu, as described previously (29). For analysis of cell surface CD4, MAGI cells in 60-mm dishes were transfected with pIRES-hrGFP-Vpu vectors. On day 2 posttransfection, cells were trypsinized, washed with phosphate-buffered saline (PBS), and resuspended in PBS containing 10% FBS. Cells were then stained with a phycoerythrin (PE)-conjugated mouse anti-human CD4 antibody (BD Biosciences, San Jose, CA). For analysis of cell surface tetherin, LLC-MK2 or HEp2 cells in 60-mm dishes were transfected with pIRES-hrGFP-Vpu vectors and harvested as described above. Cells were then reacted with an anti-HM1.24 monoclonal antibody (a generous gift from Chugai Pharmaceutical Co. Ltd., Chuo-ku, Japan) and stained with a secondary PE-conjugated anti-mouse Ig antibody (BD Biosciences). Stained cells were analyzed with a FACSCalibur instrument using CELLQuest software (BD Biosciences).

Prediction of the effects of amino acid substitutions on the stability of the HIV-1mt CA N-terminal domain. The three-dimensional (3-D) model of the HIV-1mt CA N-terminal domain (NTD) was constructed by homology modeling using "MOE-Align" and "MOE-Homology" in the Molecular Operating Environment (MOE) (Chemical Computing Group Inc., Quebec, Canada) and refined as described previously (19). The crystal structure of the HIV-1 CA NTD at a resolution of 2.00 Å (Protein Data Bank [PDB] accession number 1M9C) (37) was used as the modeling template. The changes in the stability of the CA NTD by mutations were computed by using the Protein Design application in MOE. Single-point mutations on the CA protein were generated, and ensembles of protein conformations were generated by using the LowMode MD module in MOE to calculate average stability using Boltzmann distribution. Finally, the stability scores of the structures refined by energy minimization were obtained through the stability scoring function of the Protein Design application.

Structural modeling of the Vpu TM domains. We first constructed 3-D structural models for monomers of Vpu TM domains encoded in three HIV-1mt clones (MN4/LSDQ, MN4/LSDQdtu, and MN4/LSDQgtu) with PyMOL on the basis of the previously reported structure of the HIV-1_{BH10} Vpu TM domain (PDB accession number 1PI8) (38). The HIV-1_{BH10} Vpu TM domain has a sequence identical to that of the MN4/LSDQ Vpu TM domain. The 3-D structures of their tetramers were then predicted from the constructed monomer structures with Rosetta 3.4 (39). We performed symmetry docking and predicted 10,000 tetramer structures for each molecule. Among the predicted structures, the structure with the best total score was selected as the model of the respective molecules. We compared the predicted tetramer structure of the MN4/LSDQ Vpu TM domain with the nuclear magnetic resonance (NMR) structure of the tetramer of the HIV-1_{BH10} Vpu TM domain (PDB accession number 1PI8). Their overall structures were highly similar. The root mean square deviation of C-α atoms between them was 1.64 Å.

RESULTS

Sequence homology- and structure-based modifications led to the identification of HIV-1mt CA residues that are responsible for the enhancement of viral growth in RhM cells. TRIM5 proteins inhibit retroviral infection in a species-specific manner. The RhM *TRIM5* coding sequence is highly polymorphic, and common RhM *TRIM5* alleles (*Mamu-1* to *Mamu-7*) can be divided into three groups based on polymorphisms at amino acid positions 339 to 341 within the B30.2/SPRY domain: $TRIM5^{TFP}$ (*Mamu-1* to *Mamu-3*), $TRIM5^{Q}$ (*Mamu-4* to *Mamu-6*), and $TRIM5^{CypA}$ (*Mamu-7*) (35, 40, 41). CyM TRIM5α has a Q residue at the corresponding site ($TRIM5^{Q}$), and CyM TRIM5CypA has a CypA sequence slightly different from that of RhM TRIM5CypA (42, 43). RhM and CyM TRIM5α proteins encoded by $TRIM5^{TFP}$ and $TRIM5^{Q}$ inhibit HIV-1 infection. On the other hand, CyM TRIM5CypA, but not RhM TRIM5CypA, restricts HIV-1 replication (42, 43). We have shown previously that a CXCR4-tropic MN4Rh-3 clone evaded CyM TRIM5CypA but was susceptible to TRIM5α restriction (19) and that its replication in *TRIM5α* homozygous CyM PBMCs/individuals was strongly restricted (24). Similarly, MN4Rh-3 replicated quite well in a CyM HSC-F cell line ($TRIM5^{Q/CypA}$) but very poorly in an RhM M1.3S cell line

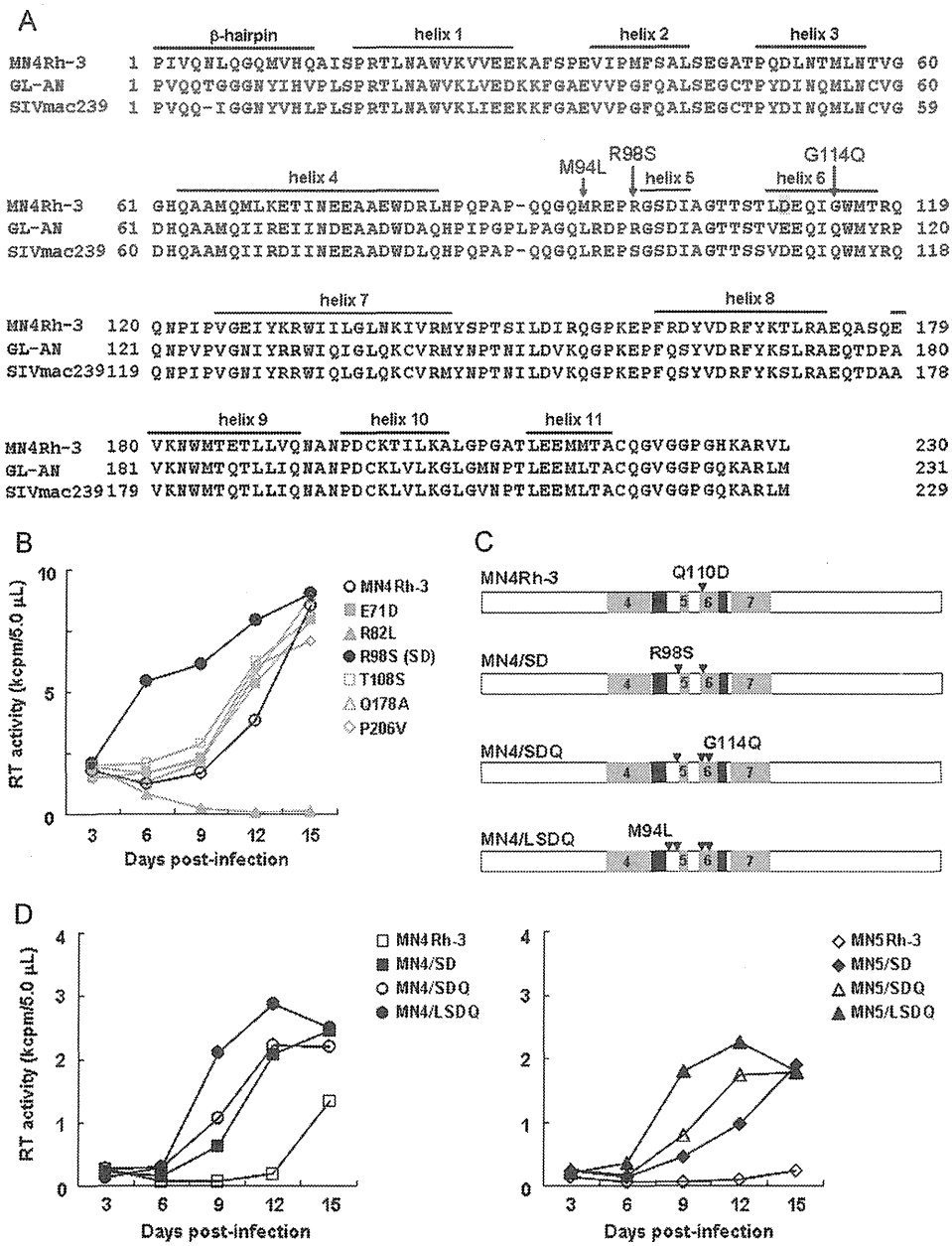

FIG 2 Identification of amino acid residues in HIV-1mt CA that are critical for viral growth enhancement in macaque cells. (A) Alignment of Gag-CA sequences. CA amino acid sequences of HIV-1mt MN4Rh-3 (19, 24), HIV-2 GL-AN (72), and SIVmac239 MA239 (71) are aligned. The N-terminal β-hairpin and helices 1 to 11 are indicated based on previously reported analyses (50, 73). The CA-Q110D mutation in MN4Rh-3 (19, 24) is shaded. Substitutions of three amino acids that contribute to the enhancement of HIV-1mt growth in macaque cells, described in this work, are indicated by arrows. (B) Growth kinetics of a parental clone, MN4Rh-3, and its CA mutants carrying a single-amino-acid change (see Table 1 for the mutants). Viruses were prepared from 293T cells transfected with the proviral clones indicated, and equal amounts (2×10^6 RT units) were inoculated into M1.3S cells (3×10^5 cells). Virus replication was monitored by RT activity released into the culture supernatants. Representative data from two independent experiments are shown. (C) Schematic CA structure of HIV-1mt clones. Amino acid substitutions are indicated in the order in which they were introduced into HIV-1mt CA. Black areas show sequences from SIVmac239. Helices 4 to 7 are shown as gray areas with the helix number. (D) Growth kinetics of CXCR4-tropic (left) and CCR5-tropic (right) HIV-1mt clones with different CA proteins (see reference 19 for CCR5-tropic MN5Rh-3). Viruses were prepared from 293T cells transfected with the indicated proviral clones, and equal amounts (2.5×10^6 RT units) were inoculated into M1.3S cells (10^6 cells). Virus replication was monitored by RT activity released into the culture supernatants. Representative data from two independent experiments are shown.

(*TRIM5*$^{TFP/TFP}$) (data not shown). Besides being a TRIM5α target, Gag-CA functions in various viral replication steps (44, 45). We thus used the M1.3S cell line as a target for multicycle infection to screen viral clones with increased replication potential following CA mutagenesis.

Modifications of MN4Rh-3 CA were performed based on sequence homology and structural modeling. As shown in Fig. 2A, the amino acid sequence identity of CA between HIV-1 and SIVmac239 is not high (~67% for SIVmac239 versus HIV-1_{NL4-3} and ~72% for SIVmac239 versus MN4Rh-3), but sequences are

relatively well conserved between HIV-2 and SIVmac239 (~90% for SIVmac239 versus HIV-2_{GL-AN}). Nevertheless, macaque TRIM5α restricts HIV-1 and HIV-2 infection but not SIVmac239. This distinct susceptibility to macaque TRIM5α results from the different CA sequences of each virus. We first selected amino acid residues in MN4Rh-3/HIV-2_{GL-AN} CA that are different from those of SIVmac239 CA and replaced these target residues with those of SIVmac239 (Table 1, MN4/SD and initial screening). The resultant clones were examined for their growth potential in M1.3S cells (Fig. 2B and Table 1). Of 25 clones tested, only MN4Rh-3 carrying an R98S change in CA (MN4/SD) exhibited enhanced viral growth efficiency (Table 1 and Fig. 2B). We previously found a growth-enhancing mutation, G114E, in CA by HIV-1mt adaptation in macaque cells (19). Since viral replication efficiency was decreased by the introduction of G114E into MN4Rh-3 (data not shown), we introduced an SIVmac239 CA-type G114Q mutation into the MN4/SD clone, and the resultant clone was designated MN4/SDQ (Fig. 2C and D). Moreover, we predicted an additional mutation that might improve the growth ability of MN4Rh-3 in macaque cells. Using HIV-2 CA, we previously found a key role of hydrogen bond formation between D97 within H4/5L (a loop between helices 4 and 5) and R119 within H6/7L (a loop between helices 6 and 7) in determining viral sensitivity to TRIM5α: TRIM5α-sensitive CA had a common H4/5L conformation with a decreased probability of hydrogen bond formation (46). The corresponding hydrogen bond was predicted to be formed between E96 in H4/5L and R118 in H6/7L of the MN4Rh-3 CA NTD. We assumed that the simultaneous introduction of SIV-CA-like amino acid residues at M94 in H4/5L and G114 in helix 6 might imitate the structural property of the SIVmac239 CA NTD surface for TRIM5α resistance and might be beneficial to improve the growth ability of MN4Rh-3 in macaque cells. The M94 residue is located in H4/5L, protruding its side chain near the G114 residue in helix 6. We therefore generated MN4/SDQ carrying the M94L mutation (MN4/LSDQ) (Fig. 2C and D). Three-dimensional locations of M94L, R98S, Q110D, and G114Q in the CA NTD are shown in Fig. 3. In addition, we constructed a series of CCR5-tropic viruses (MN5Rh-3, MN5/SD, MN5/SDQ, and MN5/LSDQ) (Fig. 2D), which carry the Env sequence derived from NF462 and a growth-enhancing Env S304G mutation (47). The growth potential of these viruses in M1.3S cells was analyzed. As shown in Fig. 2D, viral growth potential was enhanced with increasing amino acid substitutions in CA. MN4/LSDQ and MN5/LSDQ exhibited the highest replication potential in M1.3S cells in each group.

We constructed numerous HIV-1mt clones carrying CA mutations, including those described previously (48–50). All CA mutations and the growth potentials of the mutant viruses are summarized in Table 1. In the mutants derived from four HIV-1mt clones (MN4Rh-3, MN4/SD, MN4/SDQ, and MN4/LSDQ), most amino acid substitutions gave neutral or negative effects: CA amino acid substitutions that did not alter replication efficiency (L6I, E71D, T108S, Q178A, and P206V) or those that strikingly reduced the growth potential (e.g., Q50Y, T54Q, K70R, R82L, and L83Q; more than two consecutive mutations; and mutations in the β-hairpin domain). All listed HIV-1mt clones produced a significant amount of virions from transfected 293T cells, but none of them displayed a higher replication potential than MN4/LSDQ in M1.3S cells. In sum, M94L/R98S/G114Q substitutions in CA contributed to the growth enhancement of MN4Rh-3 in macaque cells.

Prediction of the effects of amino acid substitutions on the stability of the HIV-1 CA NTD. To investigate whether the M94L, R98S, Q110D, and G114Q mutations in MN4Rh-3 CA influenced the structural property of the protein, we analyzed the changes in stability by the mutations using the Protein Design application in MOE. The changes in stability by each of the point mutations M94L, R98S, Q110D, and G114Q were −0.41, 0.09, 0.25, and −1.70 kcal/mol, respectively (Fig. 3). The data suggested distinct effects of the single mutations at positions 94, 98, 110, and 114 on the stability of the HIV-1mt CA NTD. The Q110D mutation was predicted to destabilize the CA NTD. The R98S mutation has a similar negative effect on structure but to a much lesser extent. These mutations are considered to be more or less disadvantageous in terms of the CA structure. Nevertheless, they were critical for HIV-1mt growth enhancement in macaque cells (19) (Table 1 and Fig. 2). Therefore, these mutations must have given essential functions to CA protein in viral replication, which surpassed the structural disadvantage. On the other hand, M94L and G114Q mutations were predicted to stabilize the CA NTD. Therefore, these mutations may function as compensatory mutations that can redress structural disadvantages caused by R98S and Q110D mutations and increase growth ability in macaque cells. Our experimental data on MN4Rh-3, MN5Rh-3, and their derivatives having R98S/Q110D mutations, R98S/Q110D/G114Q mutations, and M94L/R98S/Q110D/G114Q mutations (Fig. 2) are consistent with this possibility.

Enhancement of viral replication efficiency by introduction of CA mutations (M94L/R98S/G114Q) correlates well with increased resistance to TRIM5α restriction. Some particular CA alterations (M94L/R98S/G114Q) of MN4Rh-3 markedly promoted viral replication in M1.3S cells with *TRIM5*$^{TFP/TFP}$ (Fig. 2D). Since TRIM5 proteins are potent restriction factors as species barriers (4, 8, 10) and can affect SIV transmission/replication *in vivo* (40, 51), it was expected that CA mutations (M94L/R98S/G114Q) would increase TRIM5α resistance as well as viral growth potential. To examine the effect of CA alterations on TRIM5α resistance, we carried out TRIM5α susceptibility assays using the recombinant SeV-TRIM5α expression system (36). TRIM5α resistance, as determined by this system, has been shown to be well reflected in the viral growth potential in macaque PBMCs/individuals due to the higher expression level of TRIM5α than that in feline CRFK cells stably expressing TRIM5α (19, 24). Four HIV-1mt clones (MN4Rh-3, MN4/SD, MN4/SDQ, and MN4/LSDQ) were assayed for their resistance to RhM-TRIM5α (*TRIM5*^{TFP}) and CyM-TRIM5α (*TRIM5*^{Q}), using SIVmac239 as a positive control. As shown in Fig. 4, the growth kinetics of SIVmac239 in cells expressing RhM- or CyM-TRIM5α or control B30.2/SPRY(−) TRIM5 were similar. Consistent with a previous analysis (19), MN4Rh-3 replication was strongly restricted in both RhM- and CyM-TRIM5α-expressing cells relative to that in control cells. Of note, TRIM5α resistance of MN4/SD, MN4/SDQ, and MN4/LSDQ quite paralleled their growth ability in M1.3S cells (see Fig. 2D for virus growth). While TRIM5α resistance of MN4/SD was increased relative to that of MN4Rh-3, MN4/SDQ exhibited higher resistance, especially to CyM-TRIM5α, than MN4/SD. MN4/LSDQ, which has the highest growth potential among the four HIV-1mt clones, showed the highest level of TRIM5α resistance, especially to RhM-TRIM5α. The HIV-1mt

TABLE 1 HIV-1mt CA mutants constructed in this study

Clone designation	CA mutation(s)[b]	Growth potential[c]
MN4Rh-3[a]	None (parental clone)	++
MN4/SD	R98S	+++
MN4/SDQ	R98S, G114Q	+++
MN4/LSDQ	M94L, R98S, G114Q	++++
Initial screening		
E71D	E71D	++
R82L	R82L	−
RL82LQ	RL82, 83LQ	−
T108S	T108S	++
Q178A	Q178A	++
P206V	P206V	++
PD	L6P	−
PDQ	L6P, G114Q	−
PYD	L6P, Q50Y	+
PYDQ	L6P, Q50Y, G114Q	+
PYQD	L6P, Q50Y, T54Q	+
PYQDQ	L6P, Q50Y, T54Q, G114Q	+
GG	LQ6, 7GG	−
GG-T117Y	LQ6, 7GG, T117Y	−
IGGN	LQGQ6-9IGGN	−
IGGN-T117Y	LQGQ6-9IGGN, T117Y	−
5IGGN	NLQGQ5-9IGGN	−
YD	Q50Y	−
YDQ	Q50Y, G114Q	−
YQD	Q50Y, T54Q	−
YQDQ	Q50Y, T54Q, G114Q	−
IIRDI	MLKET68-72IIRDI	−
TDA	ASQ176-178TDA	−
VNP	PGA206-208VNP	−
Mutants from MN4/SD		
L6I-S	L6I, R98S	++
YQ-S	Q50Y, T54Q, R98S	−
DS	E71D, R98S	+++
SS	R98S, T108S	+++
SA	R98S, Q178A	+++
SV	R98S, P206V	+++
SAV	R98S, Q178A, P206V	+++
DSAV	E71D, R98S, Q178A, P206V	+++
Mutants from MN4/SDQ or MN4/LSDQ		
L6I-LSDQ	L6I, M94L, R98S, G114Q	++++
YQ-LDQ	Q50Y, T54Q, M94L, G114Q	−
YQ-SDQ	Q50Y, T54Q, R98S, G114Q	−
YQ-LSDQ	Q50Y, T54Q, M94L, R98S, G114Q	−
K70R-LSDQ	K70R, M94L, R98S, G114Q	−
E71D-LSDQ	E71D, M94L, R98S, G114Q	+++
E79D-LSDQ	E79D, M94L, R98S, G114Q	++++
R82L-LSDQ	R82L, M94L, R98S, G114Q	−
L83Q-LSDQ	L83Q, M94L, R98S, G114Q	−
T108S-LSDQ	M94L, R98S, T108S, G114Q	++++
E79D-T108S-LSDQ	E79D, M94L, R98S, T108S, G114Q	++++
E127N-LSDQ	M94L, R98S, G114Q, E127N	+++
I134Q-LSDQ	M94L, R98S, G114Q, I134Q	−
LSDQN	M94L, R98S, G114Q, S148N	−
I152V-LSDQ	M94L, R98S, G114Q, I152V	+++
LSDQA	M94L, R98S, G114Q, Q178A	++++
IY-LSDQA	L6I, M10Y, M94L, R98S, G114Q, Q178A	++
YQ-LSDQA	Q50Y, T54Q, M94L, R98S, G114Q, Q178A	−
LSDQA-P159S	M94L, R98S, G114Q, P159S, Q178A	+++

(Continued on following page)

TABLE 1 (Continued)

Clone designation	CA mutation(s)[b]	Growth potential[c]
L6I-LSDQA	L6I, M94L, R98S, G114Q, Q178A	++++
DLSDQA	E71D, M94L, R98S, G114Q, Q178A	+++
L6I-DLSDQA	L6I, E71D, M94L, R98S, G114Q, Q178A	+++
LSDQAV	M94L, R98S, G114Q, Q178A, P206V	++++
L6I-LSDQAV	L6I, M94L, R98S, G114Q, Q178A, P206V	++++
YQ-LSDQAV	Q50Y, T54Q, M94L, R98S, G114Q, Q178A, P206V	−
DLSDQAV	E71D, M94L, R98S, G114Q, Q178A, P206V	+++
L6I-DLSDQAV	L6I, E71D, M94L, R98S, G114Q, Q178A, P206V	+++
Mutants of the β-hairpin domain		
DdN5	N5 deletion	−
DdN5-Y	N5 deletion, T117Y	−
SDdN5	N5 deletion, R98S	−
SDdN5-Y	N5 deletion, R98S, T117Y	−
DQdN5-Y	N5 deletion, G114Q, T117Y	−
SDQdN5	N5 deletion, R98S, G114Q	−
SDQdN5-Y	N5 deletion, R98S, G114Q, T117Y	−
LSDQdN5	N5 deletion, M94L, R98S, G114Q	−
LSDQdN5-Y	N5 deletion, M94L, R98S, G114Q, T117Y	−
QIG-S	NLQ5-7QIG, R98S	−
QIG-SDQ	NLQ5-7QIG, R98S, G114Q	−
QIG-LSDQ	NLQ5-7QIG, M94L, R98S, G114Q	−
GGN-S	QGQ7-9GGN, R98S	−
GGN-LSDQ	QGQ7-9GGN, M94L, R98S, G114Q	−
GGN-YQ-LSDQ	QGQ7-9GGN, Q50Y, T54Q, M94L, R98S, G114Q	−
L6I-YQ-LSDQ	L6I, Q50Y, T54Q, M94L, R98S, G114Q	−
IL-LSDQA	L6I, Q13L, M94L, R98S, G114Q, Q178A	−
IL-Y-LSDQA	L6I, Q13L, M94L, R98S, G114Q, T117Y, Q178A	−
IN-LSDQA	L6I, Q9N, M94L, R98S, G114Q, Q178A	−
IN-Y-LSDQA	L6I, Q9N, M94L, R98S, G114Q, T117Y, Q178A	−
IY-Y-LSDQA	L6I, M10Y, M94L, R98S, G114Q, T117Y, Q178A	−
INY-LSDQA	L6I, Q9N, M10Y, M94L, R98S, G114Q, Q178A	−
INY-Y-LSDQA	L6I, Q9N, M10Y, M94L, R98S, G114Q, T117Y, Q178A	−
INL-LSDQA	L6I, Q9N, Q13L, M94L, R98S, G114Q, Q178A	−
INL-Y-LSDQA	L6I, Q9N, Q13L, M94L, R98S, G114Q, T117Y, Q178A	−
IYL-LSDQA	L6I, M10Y, Q13L, M94L, R98S, G114Q, Q178A	−
IYL-Y-LSDQA	L6I, M10Y, Q13L, M94L, R98S, G114Q, T117Y, Q178A	−
INYL-LSDQA	L6I, Q9N, M10Y, Q13L, M94L, R98S, G114Q, Q178A	−
INYL-Y-LSDQA	L6I, Q9N, M10Y, Q13L, M94L, R98S, G114Q, T117Y, Q178A	−
Q13L-LSDQ	Q13L, M94L, R98S, G114Q	−
Q13L-Y-LSDQ	Q13L, M94L, R98S, G114Q, T117Y	−
Q13L-LSDQA	Q13L, M94L, R98S, G114Q, Q178A	−
Q13L-Y-LSDQA	Q13L, M94L, R98S, G114Q, T117Y, Q178A	−

[a] MN4Rh-3 CA was constructed by replacing the CypA-binding loop and H6/7L of HIV-1_{NL4-3} CA with the corresponding regions of SIVmac239 CA and by the additional introduction of a Q110D mutation (Fig. 1) (19, 24).

[b] Amino acid number in MN4Rh-3 CA.

[c] Viral growth potential in M1.3S cells. ++++, grows similarly to MN4/LSDQ; +++, grows more efficiently than MN4Rh-3; ++, grows similarly to MN4Rh-3; +, grows more poorly than MN4Rh-3; −, undetectable during the observation period.

clones here, except for MN4Rh-3, exhibited a tendency to have a higher level of resistance to CyM-TRIM5α than to RhM-TRIM5α (Fig. 4). It has been shown that TRIM5α proteins encoded by *TRIM5*^{TFP} are more restrictive to virus infection than are those encoded by *TRIM5*^{Q} (40). The observed tendency for TRIM5α resistance may be due to the difference between RhM-TRIM5α (*TRIM5*^{TFP}) and CyM-TRIM5α (*TRIM5*^{Q}) used in the assay. These results indicate that the enhancement of viral growth in M1.3S cells by CA alterations depends, at least in part, on the increased resistance to TRIM5α.

Virus replication capability in macaque PBMCs with different *TRIM5* alleles reflects the TRIM5α resistance of HIV-1mt clones. We have previously shown that MN4Rh-3 replicates well in *TRIM5α/TRIM5CypA* heterozygous CyM PBMCs/individuals, but its replication was restricted in *TRIM5α* homozygous CyM PBMCs/individuals (19, 24). To confirm the effect of the increased resistance of MN4/LSDQ and MN5/LSDQ against macaque TRIM5α on viral replication, we examined their replication potential relative to that of MN4Rh-3 and MN5Rh-3 in *TRIM5α/TRIM5CypA* heterozygous or *TRIM5α* homozygous macaque PBMCs.

First, we compared viral growth potentials of the clones in CyM PBMCs (Fig. 5A). Growth kinetics of MN4Rh-3 and MN4/LSDQ were similar in *TRIM5α/TRIM5CypA* heterozygous CyM